2D Functional Materials

International Edition: DOI: 10.1002/anie.201502009
German Edition: DOI: 10.1002/ange.201502009

Synthetic Covalent and Non-Covalent 2D Materials

*Charlotte E. Boott, Ali Nazemi, and Ian Manners**

Keywords:
block copolymers · functional materials · nanoparticles · self-assembly · two-dimensional materials

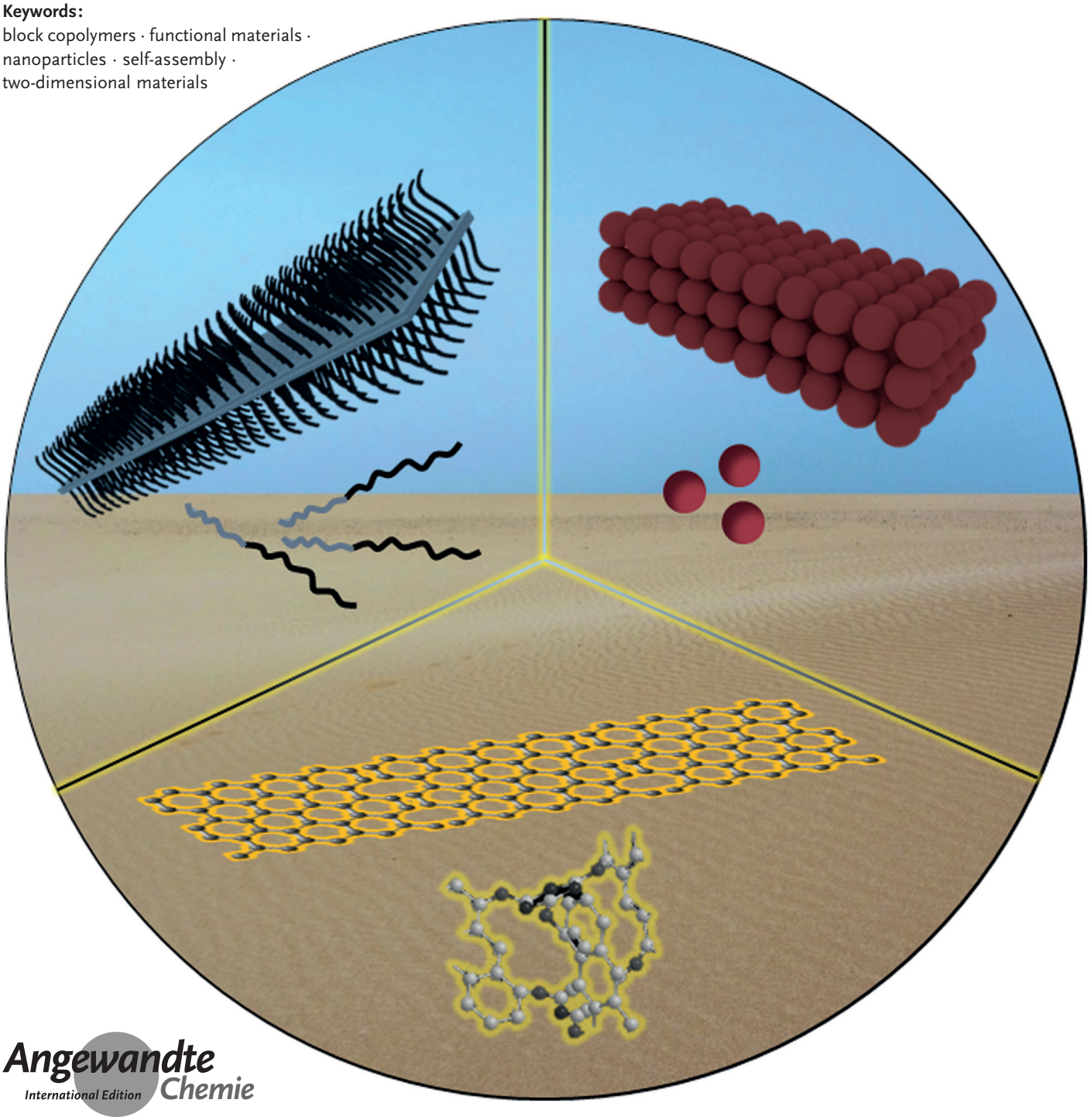

The creation of synthetic 2D materials represents an attractive challenge that is ultimately driven by their prospective uses in, for example, electronics, biomedicine, catalysis, sensing, and as membranes for separation and filtration. This Review illustrates some recent advances in this diverse field with a focus on covalent and non-covalent 2D polymers and frameworks, and self-assembled 2D materials derived from nanoparticles, homopolymers, and block copolymers.

From the Contents

1. Introduction to 2D Materials

We live in a Universe with three spatial dimensions and, over billions of years, the natural world has emerged as a myriad of simple and complex chemical structures with one, two, or three dimensional (1D–3D) atomic arrangements. Significantly, on the small length scale of under 10 nm, chemists have made impressive progress with respect to the synthesis and study of molecules and materials. This is illustrated by the cases of, for example, 1D linear polymer chains, 2D planar porphyrin, phthalocyanine, and hexabenzocoronene molecules, and 3D dendritic macromolecules. However, the generation of larger structures, especially on the length scale of 10 nm–10 μm, presents a new set of challenges.[1,2] Much recent success has been achieved with respect to the preparation of 1D and 3D nanomaterials in this size regime. Thus, 1D structures, such as nanotubes, nanowires, and nanorods, with applications in the fields of electronics, photonics, and biology have been the subject of major advances.[3] Furthermore, 3D nanoparticles that are derived either from "hard" matter (e.g. semiconductors, metals, and magnetic materials) or from "soft" materials, as exemplified by spherical micelles and vesicles from the solution self-assembly of block copolymers, have been extensively investigated.[4–7] In contrast, although the fabrication of ultra-thin films by methods such as Langmuir-Blodgett troughs,[8,9] layer-by-layer assembly,[10,11] chemical vapor deposition,[12,13] atomic layer deposition,[14,15] and molecular beam epitaxy,[16,17] has been very well-established, the development of synthetic approaches to 2D structures has generally lagged considerably behind that for their 1D and 3D analogues.

Graphite (Figure 1 a)[18] and hexagonal boron nitride consist of stacked infinite layers of fused six-membered rings (Figure 1 b,d)[19,20] and, together with layered silicates and aluminosilicates (such as clays and mica), these solids generally provide the first exposure to materials with an underlying 2D extended structure during our scientific education. Exfoliation to create individual, atomically thin 2D films of thickness less than 1 nm has led to important advances. This is especially true for graphite where, as first demonstrated in 2004, exfoliation results in the isolation of graphene (Figure 1 c).[21–23] This fascinating 2D material has led to a range of new technological opportunities, especially as a result of the remarkable electronic properties that mainly arise from quantum confinement effects. More recent developments in this area include the formation of nanostructured graphenes, such as nanoribbons (width $\geq$ ca. 2 nm) and

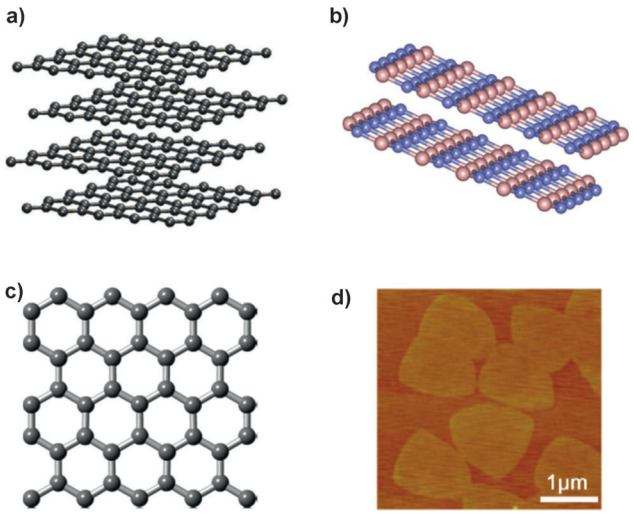

Figure 1. Structures of a) graphite, reproduced with permission from Ref. [18]; b) layered hexagonal boron nitride, reproduced with permission from Ref. [19]; and c) graphene. d) SEM image of triangular hexagonal boron nitride. Reproduced with permission from Ref. [20].

discotic liquid crystals.[24–26] Another highly productive route to prepare ultrathin 2D structures involves surface-confined self-assembly of molecules and coordination complexes, as revealed by techniques such as scanning tunneling microscopy (STM).[27–34]

In addition to the formation of ultra-thin 2D materials, crystallizable homopolymers can generate 2D platelet-shaped crystals of thickness around 5–10 nm from solution. In the

[*] C. E. Boott,[+] Dr. A. Nazemi,[+] Prof. I. Manners
School of Chemistry, University of Bristol
Bristol, BS8 1TS (UK)
E-mail: ian.manners@bristol.ac.uk

[+] These authors contributed equally to this work.

case of block copolymers, self-assembly in a selective solvent in which a crystallizable block is insoluble can generate 2D platelets of greater thickness (ca. 20–100 nm) as a result of the presence of the solvated complementary block. Initial approaches to the creation of 2D synthetic polymeric materials involved polymerization of difunctional monomers into thin films at surfaces and interfaces or other confined spaces to give cross-linked ultra-thin films.[35–37] An important contribution in the early 1990s was the report by Stupp and co-workers that involved the preparation of bilayer 2D polymers of uniform thickness (5 nm). The approach used involved the preorganization of chiral oligomers to form bilayers containing two different polymerizable groups which led to polymerization within specific planes.[38,39]

For this Review, a 2D material is defined as one in which the extent in the *z* dimension, or thickness of the material, is at least an order of magnitude smaller than the extent in the *x* and *y* dimensions. In practice, for the materials discussed in this Review, the thickness can vary from atomically thin that is, under 1 nm (as in graphene, for example) to 20–100 nm for platelet micelles formed by block copolymers. With this definition in mind, this Review illustrates some of the exciting advances in the broad field of synthetic 2D materials by means of a discussion of selected, but representative examples of work from the recent literature. The focus of the Review is on the areas of synthetic covalent and non-covalent organic and metal–organic 2D frameworks, 2D organic polymers, and also self-assembled materials derived from nanoparticles, homopolymers, and block copolymers as building blocks.

2. Synthetic, 2D Covalent and Coordination Polymers from the Polymerization of Molecular Building Blocks

2.1. Introduction

The impact of synthetic polymers on everyday life is evidenced by the production of hundreds of millions of tons of these materials per year. The recent development of advanced controlled polymerization techniques involving ionic,[40,41] radical,[42–47] and metal-catalyzed,[48] as well as ring opening-metathesis polymerization[49] methods has enabled access to well-defined linear and branched polymers and block copolymers with a wide range of useful properties and functions. On the other hand, the development of methods to extend polymer topology to 2D architectures has been much slower to emerge. Owing to their unique structural features, 2D materials offer additional potential opportunities for applications compared to their 1D analogues. For instance, such 2D structures can display well-defined pores with precise shape and size which, in turn, enhances their surface area and results in their extremely low densities. These features offer immense potential for applications as membranes and nanosieves,[50,51] and in sensing and catalysis,[52] optoelectronics,[53] stem-cell regulation,[54] gas separation,[55] formation of chiral surfaces,[56] and in the construction of high-performance devices for photocatalytic solar water splitting.[57] Considering the promise of these materials, scientists have been motivated to create versatile methods that allow the rational design and synthesis of 2D polymers.

In this Section we consider synthetic covalent organic and metal–organic 2D frameworks (2D COFs and MOFs) as well as synthetic 2D organic polymers. An exhaustive review of these materials is out of scope of this article. Additional coverage as well as the history of this field can be found in a number of recent Review articles and the references therein.[18,52,58] It is important to note that multiple definitions of 2D polymers exist in the literature. While in one definition a 2D polymer is considered as a covalently linked network formed by periodic bonding between monomers in two orthogonal directions as layered crystals or mono- and multi-layer films on surfaces and free standing sheets, generally this definition is much broader and includes 2D coordination networks and 2D objects without periodic bonding.[52] Additionally, in another definition, 2D polymers have only been restricted to free-standing covalent monolayer sheets.[59] As a result of the breadth of the field associated with this Section, only recent examples of 2D polymers with periodic structures will be discussed.[60] It should, however, be noted that providing convincing characterization of 2D periodicity has generally posed significant challenges. For example, as discussed below (Section 2.3), unequivocal confirmation in the case of 2D synthetic organic polymers awaited single-crystal X-ray diffraction studies.

Charlotte E. Boott was born in Nottingham. She graduated from the University of York in 2012 with an MChem honors degree with industrial experience. Her final year project: "The design and synthesis of small molecule kinase inhibitors for inflammatory disorders" was undertaken whilst on industrial placement at Cellzome Ltd, Cambridge. She then joined the Bristol Chemical Synthesis Centre for Doctoral Training and began doctoral studies in Ian Manners' group in 2013 where her work focuses on the formation of functional nanomaterials from the self-assembly of block copolymers.

Ali Nazemi grew up in Mianeh, Iran. He obtained his BSc in Chemistry from K. N. Toosi University of Technology (Iran) in 2005. He then moved to Canada and completed his MSc in Inorganic Chemistry at the University of Toronto in 2009 with Datong Song. He completed his PhD degree at The University of Western Ontario with Elizabeth R. Gillies and is currently a Marie Curie Postdoctoral Research Fellow with Ian Manners investigating the synthesis and crystallization-driven self-assembly of block copolymers with linear and dendritic segments.

2.2. 2D Covalent Organic and Metal–Organic Frameworks (COFs and MOFs)

Covalent organic frameworks (COFs) are a class of 2D polymers that are often obtained as insoluble microcrystalline powders from organic substrates. COFs are synthesized under reversible bond-forming conditions that often involve the condensation of boronic acids and alcohols. In this case, the topology of the resulting material is dictated by the shape of the monomers and their relative functional-group orientation. Such materials are suitable for applications in catalysis, gas storage, and separation. However, because such microcrystalline COF powders are often obtained under uncontrolled solvothermal conditions, their crystallites are randomly oriented. This precludes their use for the formation of well-defined 2D polymeric membranes, as surface-bound electrode materials, and as insulators.

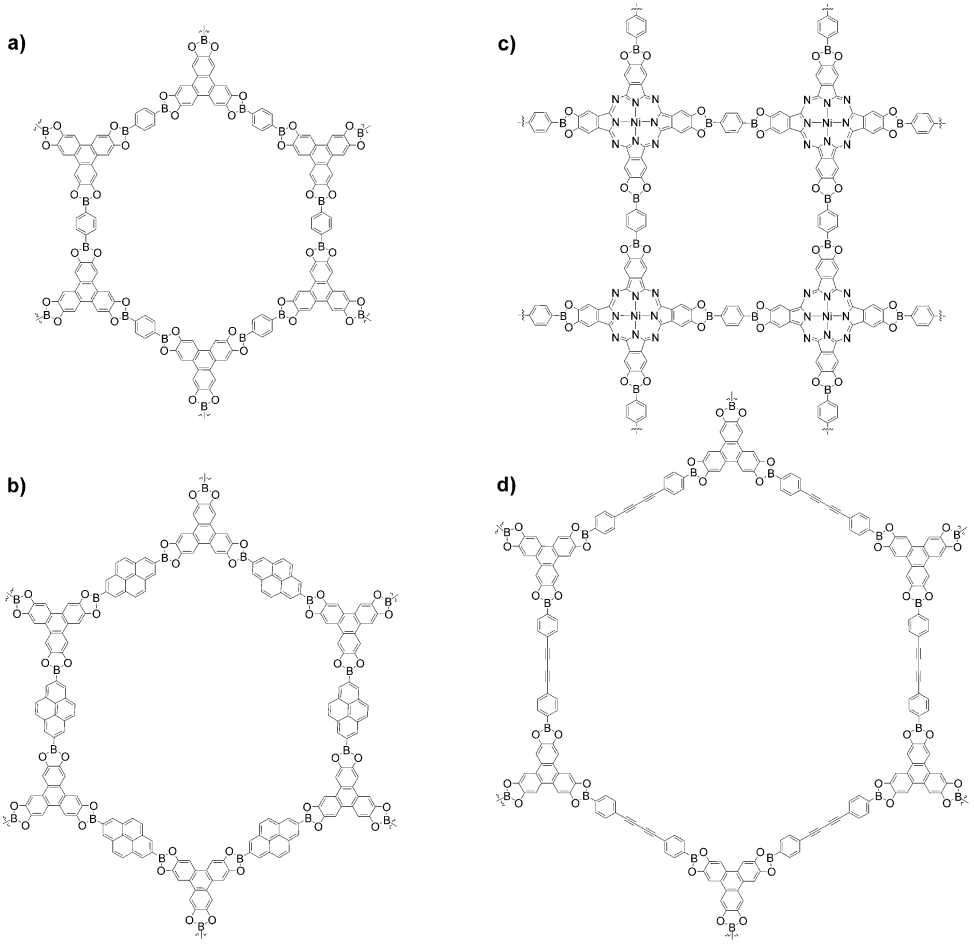

Figure 2. Chemical structures of 2D COFs used in Refs. [61, 66].

In 2011 Dichtel and co-workers reported an example of a COF thin film directly grown on single-layer graphene (SLG)-functionalized substrates under solvothermal conditions at 90 °C.[61,62] The substrates used to support SLG included copper, silicon carbide, and transparent fused silica which enabled the resulting COFs to be visualized by electron microscopy. In this study, three boronate ester-linked COFs (Figure 2a–c) were crystallized onto thin films under mixed solvent conditions. Using this method, both COF powders and thin films were obtained simultaneously. Grazing incidence diffraction studies of the films on copper-supported SLG showed that the hexagonal lattice of COF-5 (Figure 2a) obtained from solvothermal condensation of 1,4-phenylene bis(boronic acid) (PBBA) and 2,3,6,7,10,11-hexahydroxytriphenylene with pore size of 2.7 nm were oriented parallel to the substrate surface. In addition, scanning electron microscopy (SEM) revealed that the type of the underlying substrate plays an important role with respect to the thickness and uniformity of the COF-5 film obtained. It was observed that the thickness of the films on copper-supported SLG decreased from 195 ± 20 nm, corresponding to approximately 580 COF-5 layers, to 94 ± 5 nm on the transparent fused SiO_2-supported SLG, down to 73 ± 3 nm on the Si-terminated basal plane-supported SLG. Moreover, it was possible to use this technique to construct two semiconducting COF films on transparent fused SiO_2-supported SLG using triphenylene–pyrene (TP)-COF (pore size of 3.2 nm) and a Ni phthalocyanine–PBBA framework (pore size of 2.3 nm; Figure 2b and 2c respectively). It was also noted that the hexagonal symmetry of the COFs was not necessary to construct such films as the Ni phthalocyanine–PBBA framework lacked such a feature. It should also be noted that other examples of such square-grid-type 2D structures formed on surfaces include those based on tetra(4-bromophenyl)porphyrin,[63] aromatic

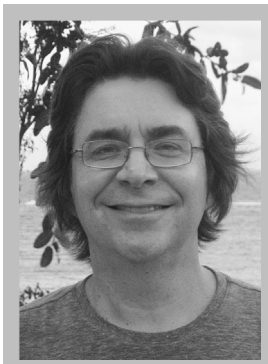

Ian Manners was born in London (UK) in 1961, and completed his PhD at the University of Bristol with Prof. Neil G. Connelly After postdoctoral work in Germany and the USA with Prof. Peter Paetzold and Prof. Harry R. Allcock he joined the University of Toronto (Canada) as an assistant professor in 1990; he became full professor in 1995 and received a Research Chair in 2001. In 2006 he returned to his Alma Mater to take up a Chair in Inorganic, Macromolecular, and Materials Chemistry. He is an elected member of the National Academies of Science of Canada (FRSC, 2001) and Britain (FRS, 2011).

Schiff base formation between various multifunctional amine- and aldehyde-containing monomers,[64] and other types of metallophthalocyanines.[65]

The same group was also able to synthesize a 2D COF by the condensation of 2,3,6,7,10,11-hexahydroxytriphenylene and 4,4′-diphenylbutadiynebis(boronic acid) onto transparent fused SiO_2-supported SLG with the largest pore size reported for a 2D COF system of 4.7 nm (Figure 2d).[66] This pore size spans over the mesoporous regime which enables the use of such 2D materials as potential hosts for polymeric and inorganic guest molecules. Molecular dynamics and density functional theory (DFT) calculations showed that, unlike other similar materials, adjacent 2D layers were not entirely eclipsed and instead were horizontally offset by 1.7–1.8 Å.[67]

In addition to the above-mentioned 2D networks that are based on covalent bond formation between their building blocks, highly ordered crystalline coordination polymers, known as metal–organic frameworks (MOFs),[68–71] have also been investigated as 2D synthetic targets. MOFs are non-covalent systems based on reversible and dynamic coordination bond formation between metal ions and their ligands. As with COFs, this leads to both advantages and disadvantages. Reversibility, and the equilibrium nature of the bond formation under the conditions used for their synthesis, can potentially give rise to "self-healing" properties for these systems and eventually result in the formation of defect-free structures. On the other hand, the same factors can potentially compromise the mechanical properties of the resulting sheets as their bond strength is often weaker than those obtained by covalent bond formation. Regardless of this potential drawback, a considerable amount of effort has been devoted to the development of MOF-based 2D structures.[72–76]

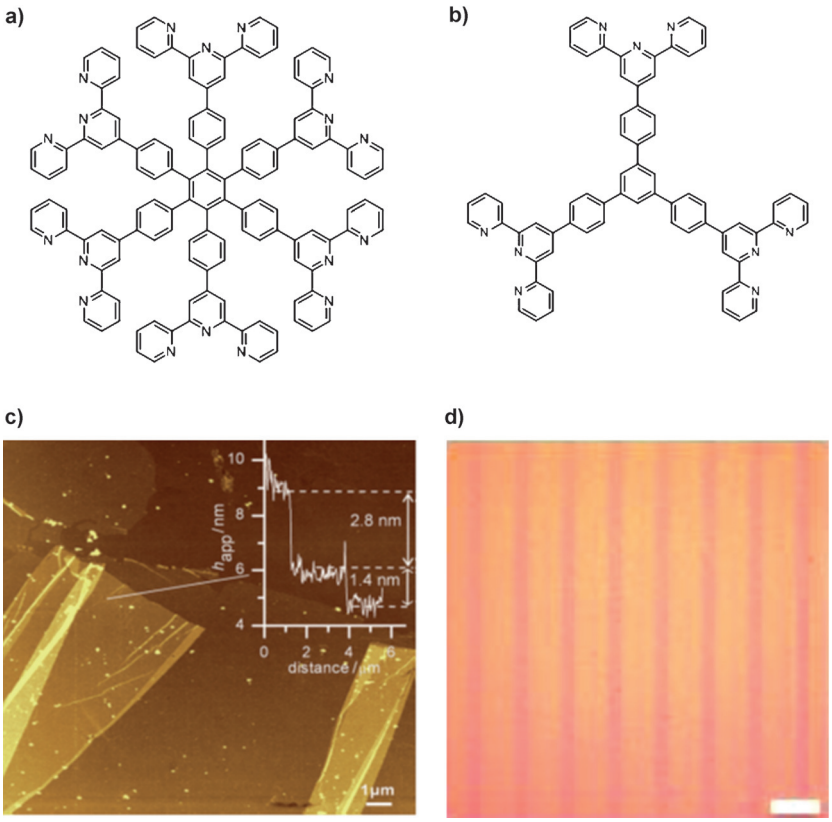

Figure 3. a) and b) chemical formula of monomers used in Refs. [77–81]. c) AFM tapping-mode image of the monolayer formed by the hexafunctional tpy-based monomer and Fe^{2+} ions with its corresponding height profile. Reproduced with permission from Ref. [77]. d) Optical microscopy of the 2D analogue of a block copolymer obtained from the hexafunctional tpy-based monomer and Zn^{2+} as well as Fe^{2+} metal ions. Scale bar 100 µm. Reproduced with permission from Ref. [81].

In a novel approach by Sakamoto, Schlüter, and their coworkers, a hexafunctional terpyridine (tpy)-based monomer (Figure 3a) was used to obtain a metal–organic free-standing sheet.[77,78] The monomer had a D_{6h} symmetry and the addition of metal ions allowed the formation of extended structures. To prevent the growth of the resulting coordination polymer in 3D, they performed the polymerization in the confined space of the air/water interface on a Langmuir–Blodgett trough. After screening a variety of metal ions, the use of Fe^{2+} was found to give the most satisfactory results. Consequently, a layer of the monomer was created at the air/water interface under a moderate pressure of 2 mN m^{-1} and an iron salt was introduced to the aqueous subphase to give a final concentration of 0.1 mM and induce the polymerization. The formation of the polymer in the form of a monolayer was then confirmed by both the appearance of the UV/Vis metal-to-ligand charge transfer band and the disappearance of the fluorescence of the monomer film. The mechanical strength and homogeneity of the resulting monolayers were then examined by transferring them onto various solid substrates (e.g. quartz glass, copper, and lacy carbon grids) followed by imaging by atomic force microscopy (AFM; Figure 3c), transmission electron microscopy (TEM), and optical microscopy techniques. It was shown that the monolayers had an apparent height of about 1.3 nm, in good agreement with the value of 0.8 nm obtained for the monomer monolayer before polymerization, with macroscopic dimensions able to span over 20×20 µm^2-sized holes. Moreover, modelling studies by the same group revealed that this monomer formed a 2D network in solution upon the addition of Fe^{2+} ions, although the coexistence of small amounts of 3D defects could not be ruled out.[79]

A second monomer with three tpy units (Figure 3b) was also synthesized and incorporated into 2D MOF-based structures.[80] X-ray photoelectron spectroscopy (XPS) analysis of the resulting monolayers suggested that not all the tpy units take part in complexation. This reaction is strongly dependent on the type of the metal ions used in the polymerization with the highest number of tpy units incorporated obtained for Fe^{2+} and Zn^{2+}. In a subsequent study by the

same groups that took advantage of the equilibrium nature of these metal-organic sheets; 2D structures of the Zn^{2+} complexes were used for metal exchange reactions with Fe^{2+}, Co^{2+}, and Pb^{2+} to obtain both random and block-type 2D monolayers (Figure 3d).[81] This investigation is particularly interesting as it addresses the challenge of modifying the internal constituents of sheet-like structures by an easy-to-perform procedure by simply dipping the initial metal–organic monolayer into the solution of the metal ion of interest and subsequent rinsing with 0.1M HCl solution.

The synthesis of single-layer 2D structures with potentially useful electronic or magnetic properties has also received attention.[82–84] In a recent study by Nishihara and co-workers, an example of a conductive single-layer nanosheet based on nickel bis(dithiolene) units prepared by a bottom-up method was reported.[85] This was achieved by the reaction of nickel(II) acetate and the multichelating ligand benzenehexathiol at both liquid-liquid and gas-liquid interfaces (Figure 4a). Based on the metalladithiolene chemistry of d^8 metal ions of Group 10, the formation of square-planar coordination polymers was expected. Sheet formation at the liquid/liquid interface using dichloromethane–water system resulted in a film with a metallic luster.[85] On the other hand, a well-defined 2D MOF single layer was synthesized in a gas–liquid interface by spraying an ethyl acetate solution of benzenehexathiol onto an aqueous solution of nickel(II) acetate and subsequent aging for 2 h under an argon atmosphere. Successful transfer of the resulting sheets onto highly oriented pyrolytic graphite (HOPG) followed by AFM analysis revealed a 0.6 nm thickness confirming the single-layer nature of the nanosheet. Moreover, STM images of the sample demonstrated a hexagonal kagomé lattice for the structure (Figure 4b). XPS analysis showed that the nanosheets were composed of S, Ni, and Na (note that Na comes from Na^+ in the aqueous medium as a charge-compensating counterion). The charge on the nickel bis(dithiolene) units was found to be a 63:37 mixture of 0 and −1 which could be tuned by chemically reducing the nanosheets using 7,7,8,8-tetracyanoquinodimethane radical anion sodium salt. This was further confirmed by cyclic voltammetry studies which showed a reversible redox process at 0.21 V versus ferrocenium/ferrocene corresponding to a 0/−1 redox couple.

In a follow up study by the same group, the properties of a bulk material formed from stacked nanosheets of the aforementioned material was investigated.[86] Using the van der Pauw method under SEM control, they were able to demonstrate that this material has a high conductivity of $1.6 \times 10^2\ S\,cm^{-1}$ at 300 K. It was also possible to gain control over the oxidation state of the nanosheets through chemical oxidation (using tris(4-bromophenyl)aminium radical cation) and reduction (using 7,7,8,8-tetracyanoquinodimethane radical anion) and to fix the nickel bis(dithiolene) motif charge at 0 and −1, respectively. This level of control over the oxidation state of single-layer nanosheets makes these materials promising candidates as the first organic 2D topological insulator materials.[86,87]

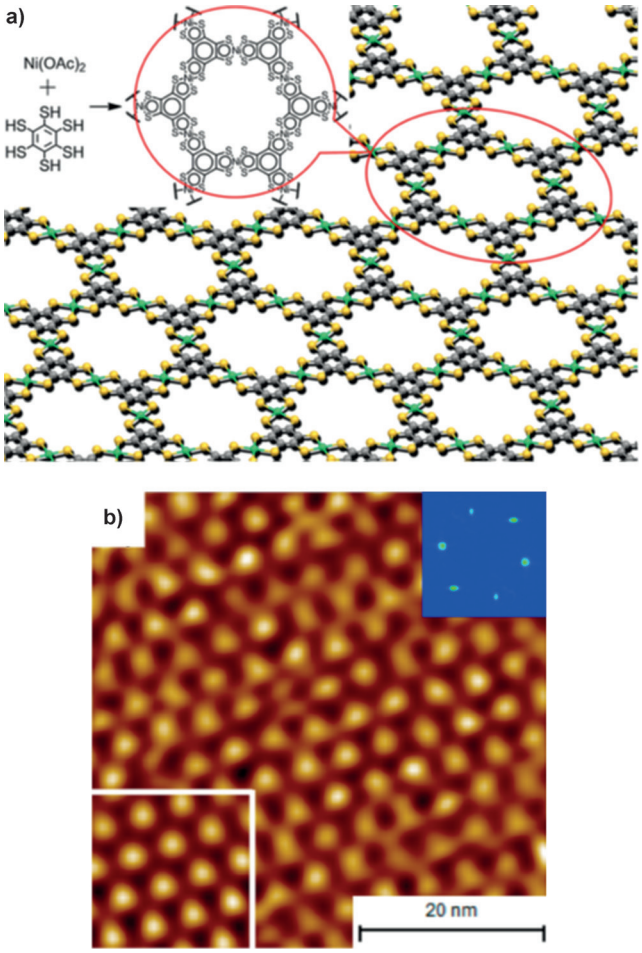

Figure 4. a) Structure of the conductive nickel bis(dithiolene) monolayer in Ref. [85]. b) STM topological image of the single layer, illustrating its hexagonal pattern. The upper-right and lower-left insets are the fast Fourier transform (FFT) and the FFT-filtered STM images, respectively. Reproduced with permission from Ref. [85].

2.3. 2D Synthetic Organic Polymers

As mentioned in Section 2.2, COFs are often prepared under reversible bond-forming conditions. In a different approach, Schlüter, Sakamoto, and co-workers synthesized an ordered 2D polymer with internal periodicity by taking advantage of the crystalline behavior of a photoreactive monomer under irreversible bond-forming conditions.[59] As shown in Figure 5a, the monomers composed of three photoreactive 1,8-diethynylanthrylene units and three terphenylene bridges, connected to each other through a benzo-1,3,5-triate unit. This design imparts a cup-shaped architecture to the molecule and promotes the desired crystal packing. Single-crystal X-ray diffraction (XRD) analysis revealed that crystals, obtained from various organic solvent mixtures as either plates or rods, have a layered rhombohedral structure in which each layer adopted a hexagonal lattice with the monomers alternating in an up and down fashion leading to conformationally enantiomeric triangular shapes (Figure 6a). Such an orientation results in the ethynyl group

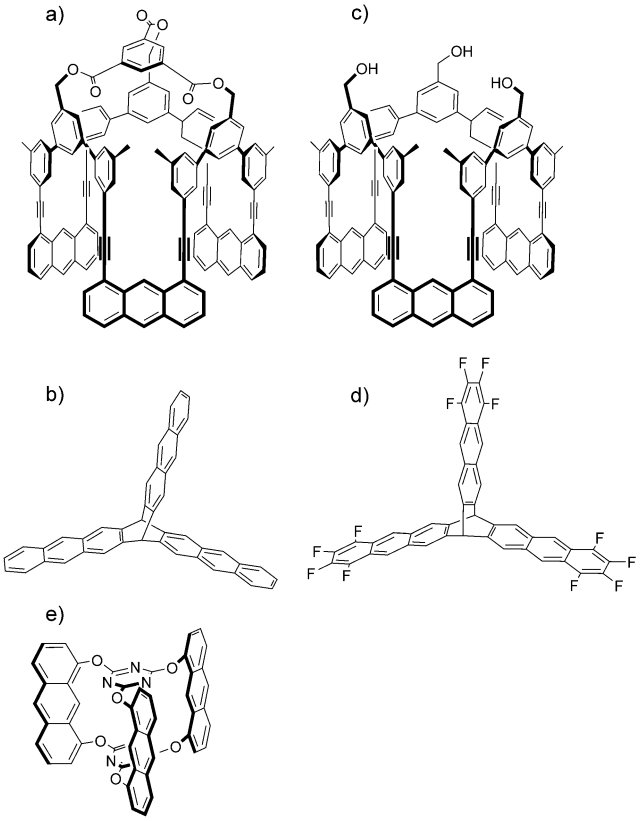

Figure 5. Chemical structures of monomers in Refs. [59, 89, 91, 93, 94] for the synthesis of 2D synthetic organic polymers.

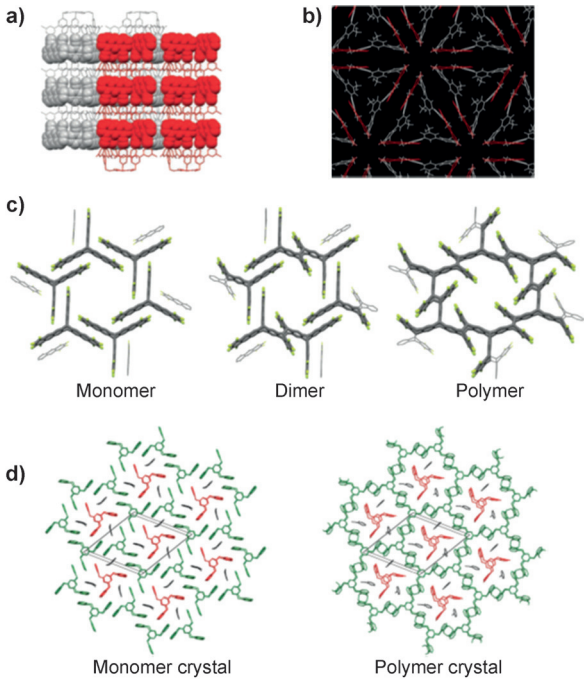

Figure 6. a) Laminar crystal structure of monomer in Figure 5a obtained by XRD showing the monomer orientation in each layer. The monomers oriented up and down are depicted in red and gray, respectively. Reproduced with permission from Ref. [59]. b) Proposed structural model of the compressed monomer in Figure 5c at the air/water interface showing the face-to-face stacking of the anthracene groups in the neighboring monomers. Reproduced with permission from Ref. [91]. c) Crystal structures of fantrip monomer, dimer, and poly(fantrip). Reproduced with permission from Ref. [93]. d) Top view of the crystal structure of the monomer in Figure 5e and its corresponding polymer. Molecules in green show the monomers participating in polymerization and those depicted in red are the ones acting as the part of the template. Reproduced with permission from Ref. [94].

of one monomer overlapping with the anthracene's 9,10-position of the adjacent monomer, which is crucial for the next step involving a [4+2] cycloaddition reaction.

This precise placement of the monomer in single crystals inhibits undesirable molecular motion and ensures an exclusive lateral polymerization. Once irradiated with 470 nm ultraviolet (UV) light, the crystals remained intact but their solid-state fluorescence was quenched, which is consistent with the successful reaction involving the anthracene units. A dramatic change in the solubility of the crystals before and after the photoirradiation was also observed. While the non-irradiated crystals were readily soluble in solvents such as 1,1,2,2-tetrachloroethane under ambient conditions, the product was hardly soluble in the same solvent at 80 °C after 1 h. These observations were suggestive of the successful polymerization of the monomer to yield a 2D structure where the pre-organization of the monomer in 2D in the crystals played an essential role. The full exfoliation to single monolayers was achieved by heating the polymerized crystals in *N*-methylpyrrolidone for 3 days. AFM analysis of the monolayer sheets not only showed a lateral dimensions of 1–2 μm but also revealed their uniform approximately 2.5 nm thickness confirming a 2D covalent topology. Moreover, a distinct electron diffraction pattern was obtained under cryogenic conditions at liquid-nitrogen temperature and this confirmed that the original crystalline order of the monomer was preserved during the polymerization process. In addition, Raman analysis of the polymer crystals confirmed the [4+2]-cycloaddition mechanism, rather than a [4+4]-cycloaddition reaction, was responsible for the polymer formation. This was evidenced by the absence of the Raman peak corresponding to the anthrylene moieties and also a decrease of the C≡C stretching signal intensity to 58% of that of the monomer crystal. However, no additional structural information for these free-standing sheets was reported in this initial report.

Sakamoto, Schlüter, King, and co-workers optimized the synthesis of antrip[88] (Figure 5b) and studied its 2D polymer formation in the solid state.[89] Antrip is a star-type molecule that has three anthraceno groups on a triptycene motif. Crystals of this compound were obtained from its benzene solution as a $P2_1/c$ polymorph. Photopolymerization was conducted by irradiation of these crystals with 400 nm UV light under N_2 atmosphere and, using a combination of deuterium-labelled antrip and spectroscopic techniques such as vibrational spectra and solid state ^{13}C NMR spectroscopy, it was confirmed that the monomer polymerization occurs by dimerization at its medial positions and thus the polymer's microstructure could be established. Strong reflections in the powder XRD spectrum of antrip and polyantrip confirmed a crystal-to-crystal transformation. Unlike the previous example (in Figure 5a), it was pointed out that because of

the fracture in single crystals during photopolymerization, this process cannot be considered as a single-crystal-to-single-crystal transformation. To obtain single sheets of the resulting polyantrip blocks, exfoliation in various solvents was then attempted. Exfoliation in *N*-methylpyrrolidone over several weeks at ambient temperature led to the production of lacy polyantrip single sheets as shown by SEM and AFM analyses. As the thermolysis of dianthracene to anthracene is well-established,[90] the lacy form of the resulting single sheets was attributed to the depolymerization of polyantrip to antrip during exfoliation process. Moreover, when these observations were analyzed in the context of tiling theory (which is concerned with tesselations of surfaces), it was possible to propose two structures for these 2D polymers that follow both honeycomb and pentaheptite lattice connectivities.

In 2014, a monomer[91] was investigated in which the benzo-1,3,5-triate unit in the structure shown in Figure 5a was removed to obtain a species with three hydroxy groups (Figure 5c) which imparts amphiphilic character to the resulting molecule.[92] This monomer was then used to study 2D polymer synthesis at the air/water interface.[91] It was hypothesized that at such an interface, the hydroxy groups would orient themselves into the bulk water while the hydrophobic part of the monomer would protrude into air, with the anthracene units having roughly uniform height above the interface. After spreading a chloroform solution of the monomer at the air/water interface, a combination of surface-pressure versus mean molecular area isotherm measurements and Brewster-angle microscopy was used to show that at a surface pressure of 20 $mN\,m^{-1}$ the monomer film had a uniform thickness. In addition, by conducting computational studies, is was shown that at such a pressure the anthracene groups of the neighboring monomers would exhibit a face-to-face stacking suitable for [4+4]-cycloaddition dimerization at their 9,10-positions (Figure 6b). Moreover, tapping mode AFM height analysis and neutron reflectivity measurements confirmed that the monomer film was in fact a monolayer with a height of about 1.7 nm. Upon irradiation with 373 nm UV light for 2 h, the fluorescent intensity of the layer was quenched leading to the assumption that the polymerization was complete with anthracene dimers being formed. AFM indentation measurements in combination with a simplified continuum mechanistic model revealed an in-plane elastic modulus of $19 \pm 7\ N\,m^{-1}$ and pre-tension value of $0.035\ N\,m^{-1}$ for the resulting 2D polymer monolayer. These values are lower than those obtained for graphene and MoS_2. When combined with fluorescence studies, these values support the molecular model for the monomer monolayer in which all the anthracene groups for neighboring monomers form pairs.

In 2014, Schlüter and King and their respective co-workers independently reported the synthesis of 2D polymers by single-crystal-to-single-crystal photopolymerization and their unequivocal structural characterization by single-crystal X-ray diffraction measurements.[93,94] Both studies took advantage of photodimerization of anthracene-based monomers by [4+4] cycloaddition. In the report by King and co-workers, a triptycene-based monomer conventionally named fantrip (Figure 5d) composed of three photoreactive tetrafluoroanthraceno "blades" connected to each other by a [2.2.2] bicyclic core, was synthesized and single crystals with either rhombohedral or hexagonal faces were obtained from chloroform.[93] Single-crystal XRD measurements on the monomer revealed a 3.63–3.71 Å length range between the face-to-face stacked anthracene blades in each layer. As noted earlier, this distance is suitable for [4+4] cycloaddition photodimerization. Interestingly, no interaction between the anthraceno blades of the neighboring layers was detected. The single crystals of poly(fantrip) were obtained by a two-step process by first irradiating the monomer single crystals with 460 nm light followed by irradiation with 400 nm light at 223 K. It was shown that initial irradiation with 460 nm light resulted in the formation of a metastable fantrip dimer which can be transformed to high quality poly(fantrip) single crystals by irradiation with 400 nm light (Figure 6c). As with the previously discussed examples, increased stability and substantial fluorescence quenching was detected suggestive of successful polymerization. Exfoliation of the resulting polymer crystals to yield thin multilayer and single sheets was achieved by their treatment with *N*-methylpyrrolidone for several days at 50 °C (Figure 7a). Interestingly, no depolymerization to the monomeric fantrip was observed during the exfoliation process. Key structural data for a single sheet 2D polymer were disclosed using single-crystal XRD analysis. It was shown that single sheets were extremely thin and porous with a thickness and pore diameter of 6.88 Å and approximately 0.9 nm, respectively. Furthermore, these 2D molecular membranes were shown to have a high pore density of about 3.3×10^{13} pore/cm^2.

In a parallel study by Schlüter and co-workers, chiral 2D polymer crystals were obtained by photopolymerization of

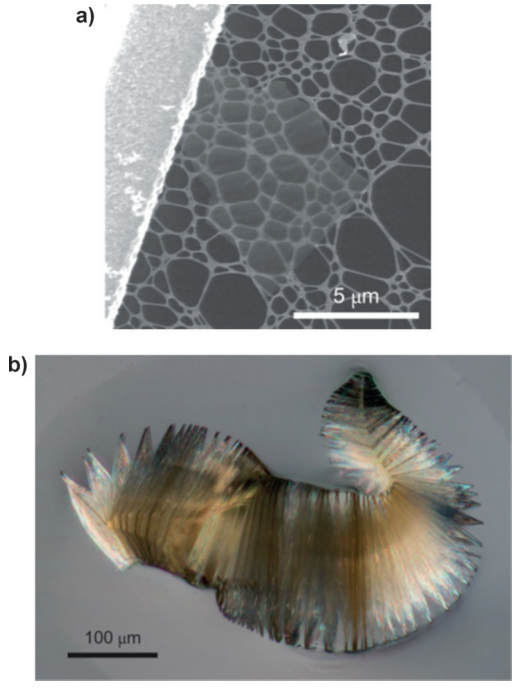

Figure 7. a) SEM image of a sheet of exfoliated poly(fantrip). Reproduced with permission from Ref. [93]. b) Polarized light microscopy image of a swollen polymer crystal during the exfoliation process. Reproduced with permission from Ref. [94].

single crystals of an enantiomorphic monomer (Figure 5e) on a gram scale.[94] Two features of this study are the unequivocal characterization of the resulting polymer single crystals by XRD analysis and the robustness of the resulting 2D polymer sheets to the extent that they could support their own weight. This is a particularly interesting property that cannot be normally achieved by molecular and supramolecular systems. As shown in Figure 5e, the monomer used was based on three photoreactive anthracene units bridged by two triazine motifs giving it a barrel-type structure. As a result of its limited degree of conformational freedom, the monomer had a low solubility, which facilitated its crystallization. Platelet-type, polyhedral, and barrel-type single crystals of the monomer could be obtained in 2-cyanopyridine by controlling the cooling rate of its boiling solution. Crystallographic data indicated that, in the crystal layers, the monomers were aligned in a fashion which allowed all the anthracene units to be stacked face-to-face in close proximity, suitable for photochemical dimerization. An interesting feature of the monomer crystal structure is that only two out of three monomer molecules take part in the photopolymerization process and the third molecule remains intact after polymerization serving as part of the template for this process (Figure 6d). Photopolymerization was then conducted by irradiation of polyhedral single crystals of the monomer with 465 nm UV light for 48 h after which a substantial decrease in the distance between the C–C bond-forming atoms of neighboring anthracene units from 3.6 Å to 1.6 Å was observed, suggesting the successful dimerization. Exfoliation of the 2D polymer single crystals to partially exfoliated crystals and, in a few cases, to single sheets was then achieved by subjecting them to *N*-methylpyrrolidone or perfluorinated carboxylic acids at 50 °C for several weeks. This exfoliation was confirmed by various microscopy techniques, such as polarized light microscopy (Figure 7b), TEM, SEM, and AFM analyses. Taking advantage of the reversible thermolytic behavior of the anthracene moiety and, using single-crystal XRD, it was possible to show that upon heating a sample of 2D polymer single crystal at 180 °C, transformation back to monomer single crystals was achievable. More significantly, this process was reversible and it was possible to cycle between monomer and polymer single crystals by UV irradiation and heating the sample.

3. Synthetic 2D Materials from the Self-Assembly of Molecular and Nanoparticle Building Blocks

Two-dimensional crystalline materials exhibit unique properties that are potentially useful for a variety of applications, such as in composites, electronics, and energy storage.[23,95–97] Nanocrystals are crystalline, 3D polyhedral or 2D polygonal structures with well-defined facets and diameters under 100 nm.[98,99] This class of materials has gained considerable interest as building blocks from which to generate self-assembled crystalline 2D materials.

The use of small discrete organic molecules to generate 2D superlattices through hydrogen bonding has been studied in depth and has been aided by the detailed structural information obtained through STM. For example, Champness and co-workers have formed 2D networks with *p*-terphenyl-3,5,3′,5′-tetracarboxylic acid adsorbed on a graphite surface.[29,31,32,100] Michaelides and co-workers have used STM, combined with infrared (IR) and DFT calculations, to determine that the structure of water–ice films on a Cu(110) substrate are composed of pentagonal arrangements of molecules instead of the previously presumed hexagonal motifs.[101] STM has also been used by Amabilino and Raval to observe the "on-surface" formation of planar macromolecules on a copper surface by using C–H activation of organic building blocks, such as perylene, pentacene, and porphyrins, to form covalently bonded structures.[102] Inorganic nanocrystals have also been deposited on a surface to form ordered structures which include the generation of honeycomb superlattices through the orientated attachment of PbSe, PbS, and CdSe single nanocrystals[103] and the formation of colloidal upconversion nanophosphor superlatices composed of $NaYF_4$ nanocrystals.[104] A detailed discussion on the formation of 2D materials at surfaces is outside the scope of this Review as their planar structure arises from the substrate rather than as an intrinsic feature of the chemistry involved. However, we will discuss the ability of nanocrystal-based systems to form 2D structures in solution in some depth.

Molecular nanoparticles are building blocks with a 3D structure that have a well-defined size, shape, and chemical composition. Their self-assembly has previously only resulted in the formation of 3D structures owing to the immiscibility of the molecular nanoparticles.[105,106] In a recent report, Zhang, Yue, Cheng, and co-workers attempted to resolve this problem through the use of Janus particles. This sub-class of molecular nanoparticles is composed of two or more distinct regions in composition and/or surface function.[107] In their study, the Janus particles had an amphiphilic structure composed of a hydrophilic ionic nanoparticle and a hydrophobic crystalline nanoparticle, with the aim that electrostatic repulsion would promote the formation of 2D nanocrystals over 3D structures.[108] To achieve this target, four sets of Janus particles were synthesized; BPOSS-Lind, BPOSS-APOSS and BPOSS-AC_{60}/DiBPOSS-AC_{60} (POSS = polyhedral oligomeric silsesquioxane; Figure 8a). The Janus particles were prepared using different coupling reactions to covalently link the two nanoparticles together. BPOSS-Lind was prepared using a palladium-catalyzed Sonagashira cross-coupling reaction whilst BPOSS-APOSS was synthesized using an amide coupling procedure. Lastly, BPOSS-AC_{60}/DiBPOSS-AC_{60} was prepared by the copper-catalyzed azide-alkyne click reaction. In each system, the butyl-functionalized POSS (BPOSS) represents the crystalline, hydrophobic nanoparticle, whereas the acetic acid POSS (APOSS), acetic acid C_{60} (AC_{60}), and Lindqvist-type polyoxometalate (Lind) represent the ionic, hydrophilic nanoparticle.

All the Janus particles successfully formed 2D nanocrystals except BPOSS-AC_{60} (Figure 8b–e) and therefore the effect of solvent, degree of ionization, and size of the molecular nanoparticles on the structure and formation of the nanocrystals could be investigated. The sheets were formed by the evaporation of a dilute solution of the molecular Janus particles where the solvent used plays a key

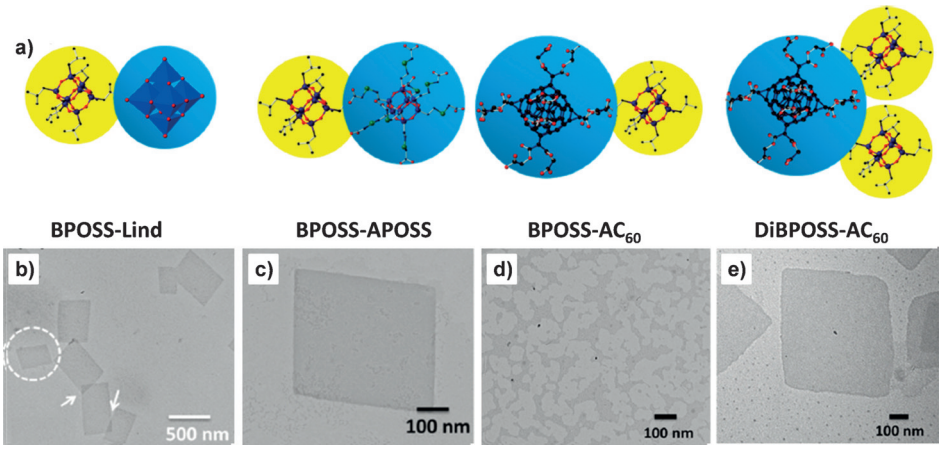

Figure 8. a) Schematic diagrams of the four Janus particles; b–e) representative bright field TEM images of the 2D nanocrystals. Adapted with permission from Ref. [108].

role in the structures obtained. A solvent with high polarity, such as *N*,*N*-dimethylformamide (DMF) and acetonitrile, was required to ensure the tetrabutylammonium counterions were solubilized. Failure to dissolve the counterions in solvents, such as acetone, resulted in the formation of 3D structures consisting of multiple layers rather than 2D nanocrystals because the repulsive interactions were reduced. The number of counterions present was also found to have a dramatic effect on the morphology obtained. In the absence of counterions, 3D crystals were obtained due to hydrogen bonding between the carboxylic acid groups, whilst the presence of too many counterions (greater than 2 per APOSS cage for BPOSS-APOSS) inhibited lateral crystal growth and resulted in fragmentation of the structures. In addition, the relative size of the two nanoparticles that comprise the Janus particles was found to be important; this needed to be similar otherwise nanocrystal formation was perturbed (Figure 8d).

However, in contrast, the size of the counterion was found to have a negligible effect on the structures obtained. The crystalline behavior of these amphiphilic Janus particles was also investigated computationally to generate phase diagrams for the formation of 2D structures with four different configurations possible; dimer, trimer, plastic, and zigzag.[109] The structures obtained were dependent on the relative size of each distinct region, pressure, and the attraction strength between the molecular nanoparticles. Janus particles of this type might be used for composite reinforcement as well as in medical and catalysis applications.

A range of metal-containing compounds which include PbSe,[103] CdSe,[110] and $NaYF_4$[104] can form nanocrystals with ligands, such as oleic acid, to stabilize their structure in solution. These compounds can exhibit interesting electronic and optical properties with lanthanide-doped nanophosphors, such as $NaYF_4$, and have possible applications in bioimaging. Furthermore, other examples of metal-containing 2D materials have begun to emerge, such as transition-metal dichalcogenides, which, when combined with organic materials, such as graphene and polyaniline nanowires, generate hybrid materials that exhibit promising optical and electronic behavior.[111–115] Recent work by Glotzer and Murray employed lanthanide fluorides (LnF_3) to synthesize nanocrystals which were obtained through the thermal decomposition of lanthanide trifluoroacetate with lithium trifluoroacetate or lithium fluoride salts in the presence of oleic acid (Figure 9a).[98] LnF_3 can form a range of monodisperse nanocrystals with the morphologies acquired being a function of the ionic radius of the metal as this affects the LnF_3 phase stability. Three different nanoplate morphologies were accessed for the

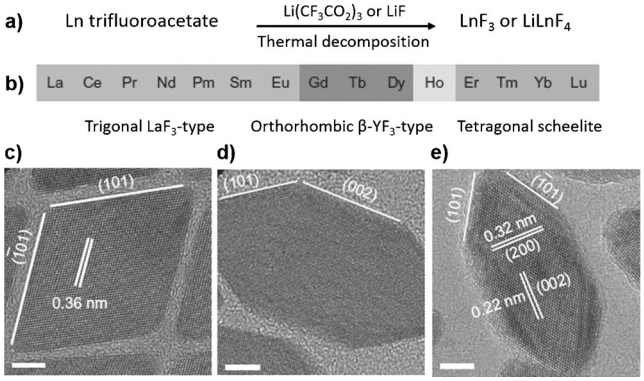

Figure 9. a) Schematic representation of the synthesis method; b) general trend of stable phases from trigonal LnF_3 to orthorhombic LnF_3 and to tetragonal $LiLnF_4$ phases as a function of the type of lanthanide ions; c–e) HRTEM images of c) TbF_3, d) DyF_3, e) EuF_3. Scale bars in (c) and (e) 5 nm; (d) 10 nm. Adapted with permission from Ref. [98].

lanthanide fluorides (Figure 9b); circular (La to Sm), irregular hexagonal (Eu to Dy; Figure 9c–e), and tetragonal bipyramidal (Er to Lu). The orthorhombic β-YF_3 irregular-hexagonal nanoplates were analyzed by high-resolution transmission electron microscopy (HRTEM) which showed the presence of two side facets in the middle of the hexagonal structure. These separate four equivalent edges form the tips of the irregular-hexagonal morphology (Figure 9e). Alteration of the lanthanide and the growth conditions resulted in a change in the nanoplate lateral dimensions.

Treatment of the rhombic and irregular-hexagonal nanoplates with *n*-hexane, whilst deposited on a viscous ethylene glycol subphase, resulted in the formation of ordered sheets where the nanoplates act as tiles. Computational analysis was carried out to analyze the mechanism of self-assembly of the structures. It was found that as the *n*-hexane evaporates, the nanoplates become closer together until the distance between them is sufficient for the oleic acid tethers to interact. At this point, nanosheets begin to form.

An alternative approach that has been successfully employed to prepare nanosheets from metal-containing

nanocrystals involves the use of nanowires as precursors.[116–118] For example, AuAg nanosheets have been prepared from AuAg nanowires and the polymer Pluronic 123.[118] Interestingly, the resulting material exhibited write-once-read-many-times memory behavior, which highlights the possible applications of such materials in data storage.

4. Synthetic 2D Materials from the Self-Assembly of Homopolymers and Block Copolymers

4.1. Platelet Crystals from Crystalline Homopolymers

Another class of materials that can form uniform 2D nanocrystals are polymers.[119,120] The growth of polymer crystals is a complex process as it requires the organization of polymer chains which involves chain diffusion and chain folding.[121] Over the past 50 years, self-seeding has emerged as one of the best methods to produce uniform 2D polymer crystals.[122] Self-seeding utilizes the fact that when a polymer crystallizes, domains with different levels of crystallinity are formed, which produces a crystal with a broad melting point. This property arises for polymer crystals because, unlike small molecules, polymers find it difficult to crystallize as they arrive at the nucleation site as a structure (Figure 10). Therefore, if the rate of growth is high, there is little time for the chains to reorganize into the optimum configuration which results in the production of a crystal with a high level of chain folding and low crystallinity. This variation in order and the degree of crystallinity throughout the polymer crystal results in different regions of the same crystal effectively possessing different melting points.

Self-seeding comprises two steps. The first involves heating a crystalline polymer sample to just below its melting point. At this temperature, molten and crystalline regions coexist and the regions with the highest levels of crystallinity survive the melting process. The second step involves cooling the sample. During this process the remaining crystallites can act as initiation sites for the growth of the polymer chains, which were dissolved in the heating process, and single crystals of uniform size and shape are prepared. However, definitive knowledge about the mechanism of the process was not available until Xu and Hu and co-workers demonstrated in 2009 that they were able to regenerate crystals (clones) that have the same orientation as the starting single crystals.[123] This correlation was confirmed using lamellar single crystals on an amorphous surface and involved the use of seed crystals with a known thermal history (Figure 11). For this study, the crystalline-coil block copolymer poly(2-vinyl pyridine)-*b*-poly(ethylene oxide) (P2VP-*b*-PEO) was used, where P2VP is the amorphous block and PEO is crystalline which is known to undergo self-seeding, and the homopolymer poly(ferrocenyldimethylsilane) (PFS).

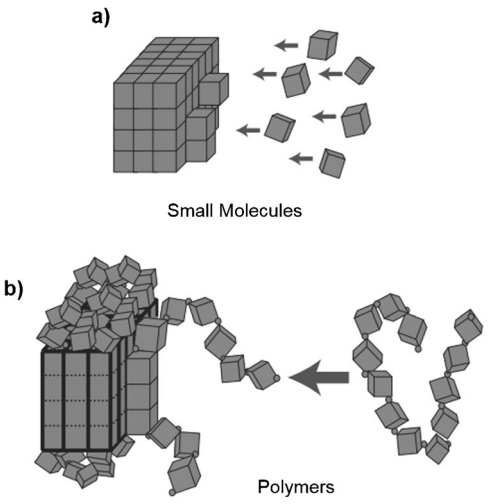

Figure 10. Schematic representation of the difference in crystallization behavior of a small molecule and polymer chain. a) Illustrates how small molecules easily pack into a crystalline structure and b) illustrates how packing polymer chains into a crystalline structure is much more challenging. Reproduced with permission from Ref. [123].

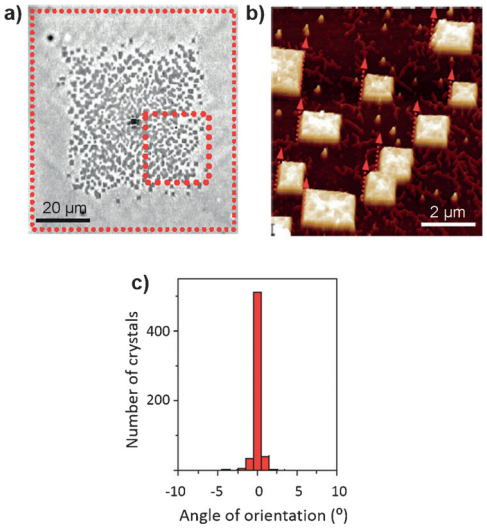

Figure 11. a) A P2VP-*b*-PEO crystal annealed for 20 s at 62 °C before it was recrystallized for 3 min at 56 °C and then quenched at room temperature; b) AFM image of the selected regions of sample (a), the red arrows indicate the orientation of the seeding crystal; c) probability of orientation of the cloned crystals with respect to the seeding crystal. Adapted with permission from Ref. [123].

In their study, the researchers were able to show that the preservation of the orientation of the crystals is a consequence of the regions of highest crystallinity surviving the annealing process and then acting as seeds for the dissolved polymer chains (unimers). This result disproved the alternative hypothesis that all polymer chains are dissolved, but those that dissolved last remember their orientation prior to melting—a phenomenon known as melt memory. The self-seeding approach provides a facile route to generate a large number of uniform polymer crystals with orientational order that can be applied to both homopolymers and crystallizable block copolymers.

Li and co-workers used the self-seeding approach to form nanosheets from thiol-terminated PEO homopolymer in solution (Figure 12).[124] The free thiol groups were employed

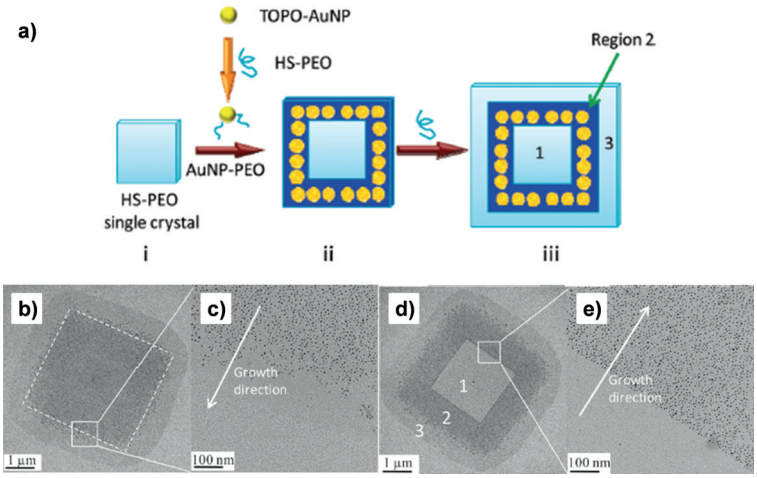

Figure 12. a) Schematic diagram of the growth mechanism of nanosheets patterned with AuNPs; b–e) TEM images of AuNP patterns formed on PEO-SH single crystals by varying addition time; gold colloid was added to PEO-SH solution at b) $t = 0$ min; d) $t = 30$ min. c) and e) show enlarged images of parts (b) and (d), respectively. Adapted with permission from Ref. [124].

to incorporate gold nanoparticles and to thereby generate nanopatterned 2D structures.[125] It was found that tri-*n*-octylphosphine oxide-protected gold nanoparticles (TOPO-AuNPs) react with PEO-SH unimer preferentially over the crystallized PEO-SH polymer; this was postulated to be a result of steric hindrance. This discovery enabled the generation of nanopatterned structures as the polymeric PEO-SH material that had already crystallized showed no reactivity towards the TOPO-AuNPs. Therefore, by varying the time between the addition of the PEO-SH polymer and the TOPO-AuNPs different 2D patterns were obtained. When PEO-SH and TOPO-AuNPs were added simultaneously, a single crystal covered with AuNPs was obtained with a peripheral region consisting of unfunctionalized PEO-SH because the AuNPs had already been consumed (Figure 12 b,c). Addition of the AuNPs 10, 20, and 30 min after the initiation of the crystallization process resulted in the formation of a frame-type structure composed of AuNPs (Figure 12 a iii, region 2, and Figure 12 d) located between an unfunctionalized center and outer border (Figure 12 a iii, regions 1 and 3 and Figure 12 d,e). As the delay time was increased, the area of the unfunctionalized inner crystal became larger. Thus, this method provides a route by which controlled nanopatterned polymer nanosheets could be obtained in which the inter-nanoparticle distance and the dimensions and location of the nanoparticle regions can be controlled. Nanoparticle-functionalized platelets with this type of structure have been shown to have applications in supported catalysis and as nanomotors.[126,127]

Although the focus of this Section has mainly been on crystalline homopolymers to generate 2D structures, non-crystalline homopolymers have also been used. For example, the work by Zuckermann and co-workers employed a sequence specific peptoid polymer, oligo-*N*-substituted glycine, to imitate the functionality and structure of proteins.[128] Nanosheets were formed in aqueous solution when two peptoid polymers of opposite charge were mixed in a 1:1 ratio. The key to the formation of the structures was the ability of the polymers to fold and their chain length. In addition, Ikeda and co-workers reported the preparation of supramolecular thiophene nanosheets from poly(phenyl-capped bithiophene)-*b*-oligo(ethylene glycol) in organic solvents.[129] The presence of the oligo(ethylene glycol) coblock was necessary to the formation of these materials as it provided the polymer with the flexibility to access the folded arrangement required to form such structures.

4.2. 2D Platelet Micelles from the Solution-Based Self-Assembly of Block Copolymers with a Crystallizable Core-Forming Block

Block copolymers (BCP) are able to self-assemble into a range of nanostructures in solution.[130] To date, the use of BCPs to generate 1D and 3D structures has been very successful but strategies for the formation of 2D morphologies have been less developed until recently.[131–137]

Composed of chemically distinct blocks that are in most cases covalently bonded together, BCPs form a solvated corona and insoluble core upon addition to a solvent that is selective for the corona-forming block. This process can provide access to a range of morphologies including spherical micelles,[131,138] vesicles,[131,139] and cylinders.[140–142] 2D platelets have also been reported.[134–137,143–146] Of particular interest for the formation of 2D structures in solution is the self-assembly of crystalline-coil BCPs by a process termed crystallization-driven self-assembly (CDSA). The crystalline nature of the core-forming block favors the formation of structures with low interfacial curvature, where a key component of the driving force for micelle formation involves the crystallization of the core.[142,143] This crystallization promotes the formation of planar structures rather than vesicles. It is also important to note that even when a crystalline core-forming block is used, the solvated corona can interfere with the crystal growth which can lead to lenticular rather than square or rectangular platelets.[147,148]

Su and co-workers employed the CDSA BCP self-assembly approach to provide a facile route to uniform platelets in solution. They prepared well-defined elongated lozenge-shaped platelets of thickness of about 15 nm from poly(2-vinylpyridine)-*b*-poly(ε-caprolactone) ($P2VP_{199}$-*b*-PCL_{310}) BCP by the addition of water to a unimer solution in DMF (Figure 13 a).[149] Attempts to prepare the platelets from an initial tetrahydrofuran (THF) unimer solution (a good solvent for both blocks) by the addition of water failed and resulted in exclusive formation of spherical micelles. This was attributed to the core-forming PCL block having a higher solubility in THF than DMF, hindering crystallization. In addition, the formation of the platelets was found to be highly temperature dependent; at 20 °C the desired lozenge-shaped crystals were obtained, but increasing the temperature to 30 °C resulted in spherical micelles. The crystal faces of the PCL homopolymer exhibit differential growth rates resulting

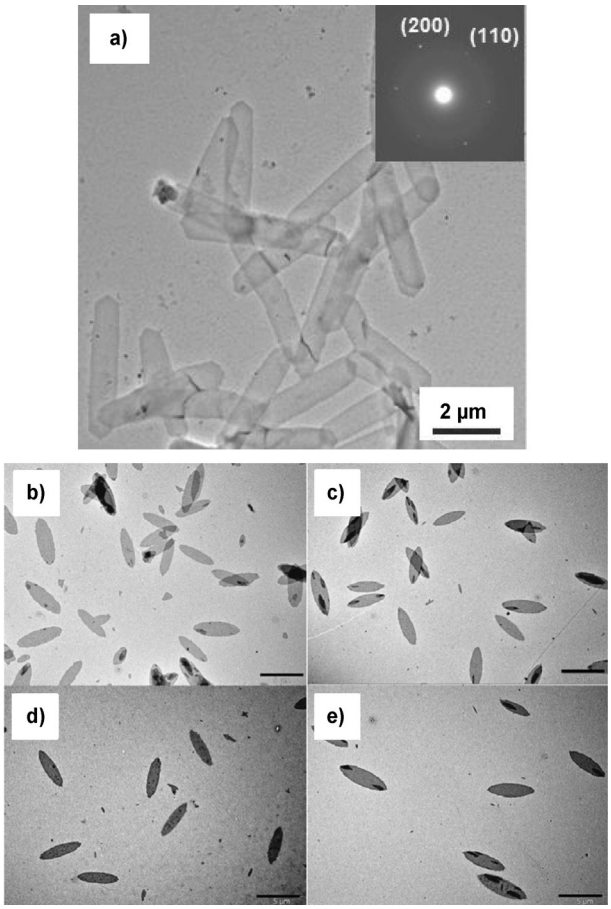

Figure 13. a) Bright field TEM images of $P2VP_{199}$-*b*-PCL_{310} plateletes formed at 20 °C in a DMF/water mixture. The inset shows the corresponding selected area electron diffraction pattern. Reproduced with permission from Ref. [149]. b–e) TEM images of polymer platelets formed by CDSA of PCL_{46}-*b*-$PDMAEMA_{25}$ for b) 1 h and c) 24 h, PCL_{46}-*b*-$PDMAEMA_{48}$ for d) 1 h and e) 24 h. Scale bars = 5 μm. Reproduced with permissions from Ref. [144].

in the formation of crystals with a high aspect ratio. The PCL-containing BCP inherits this difference and therefore the platelets produced also have a high aspect ratio. This ratio can be reduced by lowering the temperature to 10 °C, which is consistent with changes observed in PCL crystal formation at lower temperatures.

Applying the same approach, ellipsoidal platelets using a range of poly(ε-caprolactone)-*b*-poly[2-(dimethylamino)ethyl methacrylate] (PCL-*b*-PDMAEMA) block copolymers were obtained by Chen and co-workers by the addition of methanol to a unimer solution in THF at 25 °C (Figure 13b–e).[144] In this system, the PCL block forms the crystalline core and the corona is composed of PDMAEMA. Studies of a range of BCPs compositions enabled the influence of different corona and core block lengths on the micelle morphologies to be explored. The most uniform platelets were formed from the BCPs with the shorter PDMAEMA block lengths and longer PCL blocks. The platelets with a longer PCL block were more hexagonal in shape whilst the shorter PCL block length produced a more lenticular geometry. A longer corona-forming block appeared to inhibit crystal formation and to introduce defects into the structures leading to spindle-shaped platelets. A similar effect was observed for the BCPs containing shorter PCL blocks as the crystallinity of the system was reduced.

BCPs with a shorter corona-forming block are known to facilitate the formation of planar structures by minimizing chain–chain repulsion and favoring lamellar over cylindrical morphologies.[143] However, the presence of a short corona-forming block is not essential for the formation of lamellar structures. Recently, it was shown that poly(ferrocenyldimethylsilane)-*b*-poly(2-vinylpyridine) (PFS-*b*-P2VP) BCPs with block ratios of 1:6 form narrow lenticular platelets rather than cylindrical micelles in the presence of THF, a common solvent for both blocks.[148] In this system, THF appears to act as a plasticizer, facilitating crystallization of the PFS core and favoring the formation of lamellar platelet morphologies. This is consistent with the work published on PFS-*b*-P2VP BCPs with block ratios of 5:1 and 1:1 which form spherical micelles that can transform into lenticular platelets over time. However, if the initial THF concentration is greater than 30%, platelets are formed exclusively.[147]

In 2014 van de Ven and Eisenberg and co-workers successfully applied the co-assembly of PEO-*b*-PCL BCPs with PCL homopolymer to form novel 2D structures resembling rafts (Figure 14).[150] These researchers had previously reported morphological changes observed for PEO-*b*-PCL micelles over time in which the initial spheres aggregated to form rods and then, if the sample was aged for three months, ribbon morphologies were obtained. However, this process was very slow and dependent on the composition of the PEO-*b*-PCL BCP used.[151] In their new system, the addition of PCL homopolymer was found to accelerate the morphological change to lamellar structures.

A mixed solution of the BCP and PCL homopolymer was prepared in 1,4-dioxane and water was slowly added to the solution, a selective solvent for the PEO, resulting in crystallization of the PCL. It was vital that the homopolymer is added at the same time for the raft morphologies to be obtained as addition of PCL homopolymer to a solution of PEO-*b*-PCL spheres failed to generate the lamellar morphologies observed for the mixed self-assembly system. The rate of raft formation was found to be dependent on the

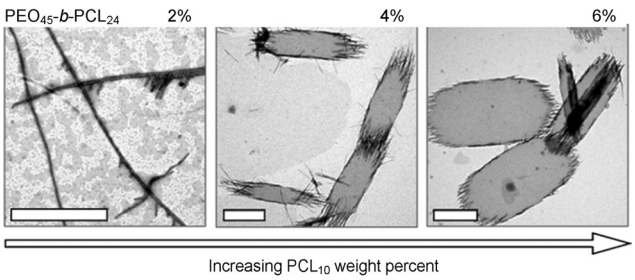

Figure 14. Morphological transformations induced by increasing amounts of PCL_{10} in the blends of PCL_{10} and PEO_{45}-*b*-PCL_{24}. TEM images show structures generated for PEO_{45}-*b*-PCL_{24} as a function of increasing PCL_{10} content. Scale bar = 2 μm. Reproduced with permission from Ref. [150].

crystallinity of the system. As a result, addition of higher amounts of PCL homopolymer resulted in the lamellar structure being formed at a higher rate. An increase in homopolymer content also resulted in rafts of larger sizes being formed. Moreover, despite the fact that the structures generated had a high polydispersity in size, their widths and lengths were found to be proportional. The proposed mechanism for the formation of the raft structures consists of several adhesion processes; the aggregation of spheres to form cylindrical micelles followed by the alignment of the cylindrical micelles to form the rafts. The cylindrical micelles that assemble to form the rafts can clearly be observed at the end of the lamellae whereas the long edges remain smooth as the cylinders orientate in a side-on manner to generate the rafts. Such an alignment mechanism to form lamellae in solution is unprecedented in 2D BCP self-assembly and highlights the potential of co-crystallization self-assembly to create 2D structures.

Despite these advances concerning the fabrication of 2D nanostructures using solution-based processing techniques, the ability to form 2D nanoobjects of controlled size in solution has not been described. However, recent work published by Manners and Winnik and by Jiang and their respective co-workers has reported the application of seeded growth to form platelets[145] and nanosheets[146] by living CDSA. Living CDSA is a process in which the ends of the micelles remain active to further epitaxial growth in an analogous manner to a living covalent polymerization by the sequential addition of BCPs with a common crystallizable core block[141,142] or different core blocks with a small lattice mismatch.[152] In 1D, this method has been employed to precisely create uniform structures of controlled size and low polydispersity through techniques such as seeded growth[142] and self-seeding,[153,154] and to generate a variety of multicompartment block co-micelles with nanosegregated functionality.[155,156] Extending this process to 2D systems is highly desirable as the resulting materials have potential applications in thermosets,[157] composites,[158–160] and as platforms for nanoparticles.[124,144,161]

Seeded growth uses short seed micelles with crystalline cores as the initiation site for further epitaxial elongation. The first seeded growth of a 2D nanostructure from a BCP was reported in 2010 using a poly(ferrocenyldimethylsilane)-*b*-poly[bis(trifluoroethoxy)phosphazene] (PFS-*b*-PP).[162] Addition of a PFS_{54}-*b*-PP_{290} unimer solution to PFS_{34}-*b*-$P2VP_{272}$ cylindrical seed micelles generated lenticular platelet micelles. Jiang and co-workers prepared nanosheets using hyperbranched poly(ether amine) (hPEA) capped with heptaisobutyl polyhedral oligomeric silsesquioxane (POSS) groups by adding water as a selective solvent to a unimer solution of the material in 1,4-dioxane (Figure 15).[146] Using fragments of the nanosheets as seeds for further growth, 2D platelets with a low polydispersity and tunable size can be formed. These seeds were generated by rapidly cooling a 1:1 water:dioxane solution of the nanosheets, that had been heated at 90 °C for 2 h, to 25 °C. Mixed functionality nanosheets were also synthesized from the random co-crystallization of hPEA capped with POSS bearing different functional groups (anthracene and ferrocene).

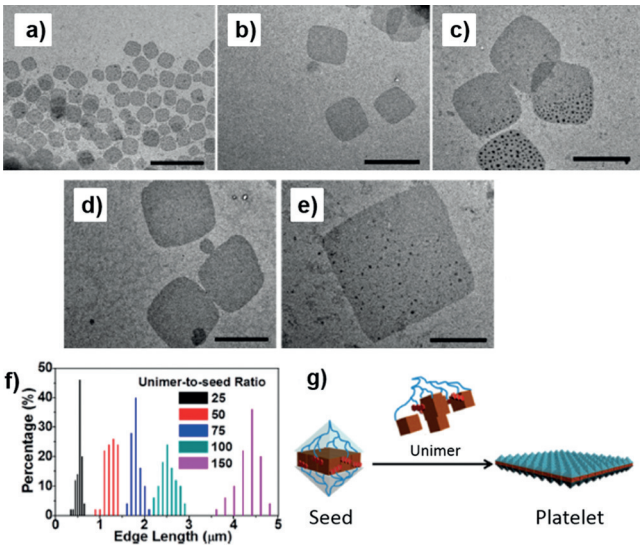

Figure 15. TEM images of the square nanosheets formed through CDSA of HP1 unimers with fragmented HP1-NSs (NS = nanosheet) as seeds at 60 °C for 24 h. The unimer-to-seed ratio is 25 (a), 50 (b), 75 (c), 100 (d), and 150 (e). The scale bar is 2 μm for all TEM images; f) Edge length distribution histograms of the nanosheets formed through CDSA with different unimer-to-seed ratios; g) The proposed mechanism for the formation of the size-tunable square platelets by CDSA from crystallite seeds. Reproduced with permission from Ref. [146].

This complements their previous work which showed that hPEA nanosheets functionalized with anthracene POSS can act as a platform for gold nanoparticles.[161] The nanosheets formed in this manner are responsive to pH, ionic strength, and temperature, with the nanosheets functionalized with gold nanoparticles having the ability to transfer reversibly between water and toluene when these parameters are altered.

Jiang's work successfully incorporated functionality into the 2D structures. The ability to spatially isolate functionality in 2D is also a very attractive target. The formation of multicompartment 2D nanostructures is currently an underdeveloped field with only a few reports of their preparation. The first report was in 2004 by Cheng and co-workers whom employed the growth of a poly(ethylene oxide)-*b*-polystyrene (PEO-*b*-PS) BCP single-crystal seeds followed by the addition of PEO homopolymer to form nanosheets with alternating rings of BCP and homopolymer.[163] In 2013, Wooley, Pochan, and co-workers used cooperative self-assembly of BCP blends to generate 2D structures with nanosegregated domains derived from the two BCPs.[164]

Previous work has shown that it is possible to use living CDSA to prepare block co-micelles with nanosegregated functionality in 1D.[155,165,166] In 2014, it was demonstrated that 2D multicompartment block co-micelles can be formed.[145] Qualitative experiments involving the addition of a range of platelet-forming PFS-based BCPs, PFS-b-polyisoprene (PFS_{76}-*b*-PI_{76}), PFS-b-poly(dimethylsiloxane) (PFS_{114}-*b*-$PDMS_{81}$), and PFS-b-poly(methylvinylsiloxane) (PFS_{69}-*b*-$PMVS_{35}$) to short cylindrical crystallite seed micelles gener-

ated by ultrasonication was investigated to determine if living CDSA could be extended into 2D (Figure 16). The area of the lenticular platelets obtained had a low area polydispersity (< 1.1) and a linear dependence with unimer-to-seed ratio (Figure 16g), indicating the living nature of the process.

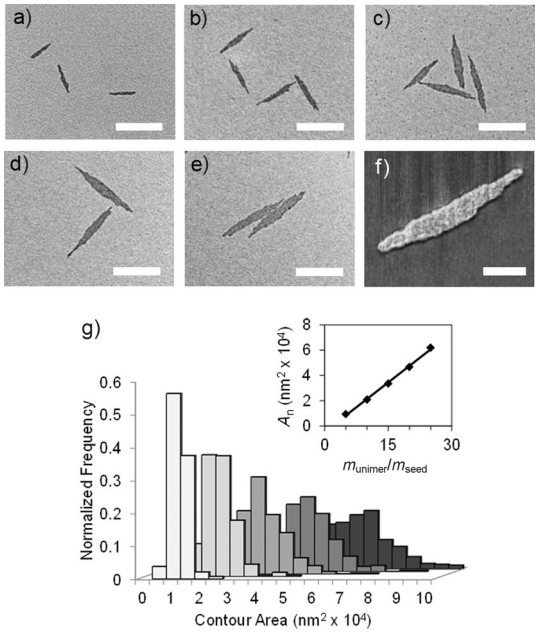

Figure 16. Monodisperse lenticular platelet micelles of controlled area by crystallization-driven self-assembly in two dimensions. a–e) TEM micrographs of PFS_{114}-*b*-$PDMS_{81}$ platelet micelles grown from PFS_{28}-*b*-$PDMS_{560}$ crystallite seed micelles (average length = 23 nm) with unimer:seed ratios of a) 5:1, b) 10:1, c) 15:1, d) 20:1, and e) 25:1 (w/w). Scale bars = 500 nm. f) AFM phase image of a lenticular platelet micelle formed from a 25:1 unimer:seed ratio. Scale bar = 300 nm. g) Histograms showing the contour area distribution of samples (a)–(e). The inset shows the linear dependence of micelle area on the unimer:seed ratio. Reproduced with permission from Ref. [145].

Further complexity can be introduced into the structures through the formation of block co-micelles by the sequential addition of the different platelet-forming BCPs with a common crystallizable core (Figure 17). To visualize the concentric structure of the micelles, BCPs of PFS_{113}-*b*-$[PDMS_{68}/PMVS_3]_{71}$ functionalized with red, green, and blue fluorescent dyes were used and laser scanning confocal microscopy (LSCM) revealed their segmented ring structure (Figure 17c,d). Combining the living CDSA in 2D with the previously established work in 1D enabled the formation of complex hierarchical structures that resembled nanoscale single- and double-headed arrows.[145] The ability to combine these self-assembly processes provides a route to control the distance between the morphologically distinct platelet regions, as well as further opportunities to generate complex hierarchical structures from soft matter.

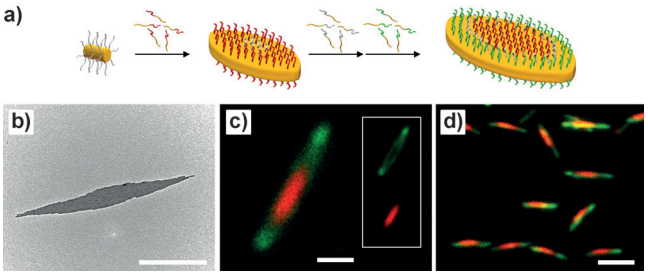

Figure 17. Growth of concentric lenticular block co-micelles in 2D. a) Schematic diagram showing the formation of concentric lenticular block co-micelles in 2D from a cylindrical crystallite seed; b) TEM image of lenticular platelet micelle formed by the sequential addition of non-fluorescent, and red and green fluorescent polymers; c) and d) LSCM images of the triblock co-micelles showing their concentric structure. Scale bars b) and c) 500 nm and d) 2 μm. Adapted with permission from Ref. [145].

5. Conclusions and Future Outlook

Although enormous impetus to the field of 2D materials was provided by the discovery of graphene, the area still remains relatively underdeveloped compared to the situation for 1D and 3D structures. As is clear from the content of this Review, a key recent theme is the use of "bottom-up" synthetic approaches to prepare 2D structures in which Ångstrom- or nanometer-size building blocks are used as precursors under mild synthetic conditions. This contrasts with the often harsh reaction procedures characteristic of the synthesis of many inorganic materials with layered structures and the "top-down" exfoliation methods that are also popular. Advantages of the "bottom-up" approach arising from the milder reaction conditions and solution processing include the ability to introduce functionality into the resulting products, achieve dimensional control, prepare segmented assemblies, and to fabricate large area films. However, this strategy presents its own set of challenges; these include favoring the formation of 2D over 1D or 3D structures, reduction of the number of defects, and the formation of free-standing 2D films in the absence of a dimension-confining surface.

The selected examples discussed herein illustrate that a wide range of "bottom-up" approaches can now be used to access intriguing "planar" forms of matter. Various small building blocks can be utilized for their construction, including small molecules, nanoparticles, homopolymers, and block copolymers. This has produced an extensive variety of new 2D materials with interesting structural and physical properties that were previously inaccessible. Detailed studies of the properties of the various new types of 2D material together with theoretical insight are necessary to enable both fundamental understanding and applied advances. A range of possible technological applications appear to offer promising opportunities for the future.

Depending on their composition and building blocks, 2D materials have a range of potential features that make them of extensive fundamental and applied interest. As illustrated with graphene and related materials, dimensional confine-

ment effects can generate remarkable optoelectronic properties that offer applications in ultrathin transistors, solar cells displays, and other devices.[167] Metal-containing nanosheets offer redox-activity, magnetism, fluorescence as well as other, potentially useful types of physical behavior.[84,85] 2D structures have an intrinsically high surface area and are therefore promising for the fabrication of sensors, porous membranes and nanosieves, and supported catalysts. Materials confined to 2D offer possible advantages over their 1D and 3D cousins for composite reinforcement, interface stabilization, and as intravascular carriers, and may provide access to unusual liquid-crystalline behavior.[168–170] The ability to generate 2D structures with spatially controlled regions of functionality has already been used to prepare platelets patterned with fluorescent dyes and with uses as magnetically separable catalysts.[124,145] Given that new and improved synthetic methods are constantly emerging, the prospects for the design and realization of functional 2D materials with enhanced structural control and complexity appear particularly bright.

C.E.B. thanks the Bristol Chemical Synthesis Centre for Doctoral Training, funded by the Engineering and Physical Sciences Research Council, for a PhD studentship. A.N. is grateful to the European Union for a Marie Curie Fellowship. I.M. thanks the EU for a European Research Council Advanced Investigator Grant.

How to cite: *Angew. Chem. Int. Ed.* **2015**, *54*, 13876–13894
Angew. Chem. **2015**, *127*, 14082–14101

[1] I. W. Hamley, *Angew. Chem. Int. Ed.* **2003**, *42*, 1692–1712; *Angew. Chem.* **2003**, *115*, 1730–1752.
[2] M. D. Ward, P. R. Raithby, *Chem. Soc. Rev.* **2013**, *42*, 1619–1636.
[3] N. P. Dasgupta, J. Sun, C. Liu, S. Brittman, S. C. Andrews, J. Lim, H. Gao, R. Yan, P. Yang, *Adv. Mater.* **2014**, *26*, 2137–2184.
[4] H.-C. Kim, S.-M. Park, W. D. Hinsberg, *Chem. Rev.* **2010**, *110*, 146–177.
[5] F. H. Schacher, P. A. Rupar, I. Manners, *Angew. Chem. Int. Ed.* **2012**, *51*, 7898–7921; *Angew. Chem.* **2012**, *124*, 8020–8044.
[6] M. Grzelczak, J. Vermant, E. M. Furst, L. M. Liz-Marzán, *ACS Nano* **2010**, *4*, 3591–3605.
[7] Z. Nie, A. Petukhova, E. Kumacheva, *Nat. Nanotechnol.* **2010**, *5*, 15–25.
[8] L. Boubekeur-Lecaque, B. J. Coe, K. Clays, S. Foerier, T. Verbiest, I. Asselberghs, *J. Am. Chem. Soc.* **2008**, *130*, 3286–3287.
[9] M. Feng, L. Gao, Z. Deng, W. Ji, X. Guo, S. Du, D. Shi, D. Zhang, D. Zhu, H. Gao, *J. Am. Chem. Soc.* **2007**, *129*, 2204–2205.
[10] G. Decher, *Science* **1997**, *277*, 1232–1237.
[11] A. Y. W. Sham, S. M. Notley, *Langmuir* **2014**, *30*, 2410–2418.
[12] P. Sutter, J. Lahiri, P. Albrecht, E. Sutter, *ACS Nano* **2011**, *5*, 7303–7309.
[13] I. Vlassiouk, M. Regmi, P. Fulvio, S. Dai, P. Datskos, G. Eres, S. Smirnov, *ACS Nano* **2011**, *5*, 6069–6076.
[14] B. Radisavljevic, A. Radenovic, J. Brivio, V. Giacometti, A. Kis, *Nat. Nanotechnol.* **2011**, *6*, 147–150.
[15] G. He, J. Gao, H. Chen, J. Cui, Z. Sun, X. Chen, *ACS Appl. Mater. Interfaces* **2014**, *6*, 22013–22025.
[16] J. Park, W. C. Mitchel, L. Grazulis, H. E. Smith, K. G. Eyink, J. J. Boeckl, D. H. Tomich, S. D. Pacley, J. E. Hoelscher, *Adv. Mater.* **2010**, *22*, 4140–4145.
[17] M. J. Manfra, *Annu. Rev. Condens. Matter Phys.* **2014**, *5*, 347–373.
[18] P. Miró, M. Audiffred, T. Heine, *Chem. Soc. Rev.* **2014**, *43*, 6537–6554.
[19] A. Pakdel, Y. Bando, D. Golberg, *Chem. Soc. Rev.* **2014**, *43*, 934–959.
[20] Y. Gao, W. Ren, T. Ma, Z. Liu, Y. Zhang, W.-B. Liu, L.-P. Ma, X. Ma, H.-M. Cheng, *ACS Nano* **2013**, *7*, 5199–5206.
[21] F. Bonaccorso, L. Colombo, G. Yu, M. Stoller, V. Tozzini, A. C. Ferrari, R. S. Ruoff, V. Pellegrini, *Science* **2015**, *347*, 41–51.
[22] For analogues of graphene based on Si, Ge, P, As, and carbon nitride see following references, respectively: a) V. O. Özçelik, S. Cahangirov, S. Ciraci, *Phys. Rev. Lett.* **2014**, *112*, 246803; b) M. E. Dávila, L. Xian, S. Cahangirov, A. Rubio, G. L. Lay, *New J. Phys.* **2014**, *16*, 095002; c) H. Liu, A. T. Neal, Z. Zhu, Z. Luo, X. Xu, D. Tomanek, P. D. Ye, *ACS Nano* **2014**, *8*, 4033–4041; d) C. Kamal, M. Ezawa, *arXiv*: 14105166v1 (2014); e) S. Zhang, Z. Yan, Y. Li, Z. Chen, H. Zeng, *Angew. Chem. Int. Ed.* **2015**, *54*, 3112–3115; *Angew. Chem.* **2015**, *127*, 3155–3158; f) G. Algara-Siller, N. Severin, S. Y. Chong, T. Bjçrkman, R. G. Palgrave, A. Laybourn, M. Antonietti, Y. Z. Khimyak, A. V. Krasheninnikov, J. P. Rabe, U. Kaiser, A. I. Cooper, A. Thomas, M. J. Bojdys, *Angew. Chem. Int. Ed.* **2014**, *53*, 7450–7455; *Angew. Chem.* **2014**, *126*, 7580–7585.
[23] K. S. Novoselov, A. K. Geim, S. V. Morozov, D. Jiang, Y. Zhang, S. V. Dubonos, I. V. Grigorieva, A. A. Firsov, *Science* **2004**, *306*, 666–669.
[24] X. Li, X. Wang, L. Zhang, S. Lee, H. Dai, *Science* **2008**, *319*, 1229–1232.
[25] A. B. Shivanandareddy, S. Krishnamurthy, V. Lakshminarayanan, S. Kumar, *Chem. Commun.* **2014**, *50*, 710–712.
[26] W. Pisula, X. Feng, K. Müllen, *Chem. Mater.* **2011**, *23*, 554–567.
[27] L. Piot, D. Bonifazi, P. Samorì, *Adv. Funct. Mater.* **2007**, *17*, 3689–3693.
[28] Y. Yang, C. Wang, *Chem. Soc. Rev.* **2009**, *38*, 2576–2589.
[29] M. O. Blunt, J. C. Russell, M. d. C. Gimenez-Lopez, N. Taleb, X. Lin, M. Schröder, N. R. Champness, P. H. Beton, *Nat. Chem.* **2011**, *3*, 74–78.
[30] M. O. Blunt, J. C. Russell, M. d. C. Giménez-López, J. P. Garrahan, X. Lin, M. Schröder, N. R. Champness, P. H. Beton, *Science* **2008**, *322*, 1077–1081.
[31] A. Saywell, G. Magnano, C. J. Satterley, L. M. A. Perdigão, A. J. Britton, N. Taleb, M. d. C. Giménez-López, N. R. Champness, J. N. O'Shea, P. H. Beton, *Nat. Commun.* **2010**, *1*, 75.
[32] A. Stannard, J. C. Russell, M. O. Blunt, C. Salesiotis, M. d. C. Giménez-López, N. Taleb, M. Schröder, N. R. Champness, J. P. Garrahan, P. H. Beton, *Nat. Chem.* **2012**, *4*, 112–117.
[33] J. Carrasco, A. Michaelides, M. Forster, S. Haq, R. Raval, A. Hodgson, *Nat. Mater.* **2009**, *8*, 427–431.
[34] S. Haq, F. Hanke, J. Sharp, M. Persson, D. B. Amabilino, R. Raval, *ACS Nano* **2014**, *8*, 8856–8870.
[35] G. Gee, E. K. Rideal, *Proc. R. Soc. London Ser. A* **1935**, *153*, 116–128.
[36] A. Dubault, M. Veyssie, L. Liebert, L. Strzelecki, *Nature Phys. Sci.* **1973**, *245*, 94–95.
[37] M. A. Markowitz, R. Bielski, S. L. Regen, *J. Am. Chem. Soc.* **1988**, *110*, 7545–7546.
[38] S. I. Stupp, S. Son, H. C. Lin, L. S. Li, *Science* **1993**, *259*, 59–63.
[39] For relevant previous work see: a) A. Blumstein, J. Herz, V. Sinn, C. Sadron, *C. R. Hebd. Seances Acad. Sci.* **1958**, *246*, 1856–1858; b) A. Blumstein, *Adv. Macromol. Chem.* **1970**, *2*, 123–146; c) T. Kunitake, *Angew. Chem.* **1992**, *104*, 692–710; d) S. Asakuma, T. Kunitake, *Chem. Lett.* **1989**, 2059–2062; e) S.

Asakuma, H. Okada, T. Kunitake, *J. Am. Chem. Soc.* **1991**, *113*, 1749 – 1755.
[40] M. Szwarc, *Nature* **1956**, *178*, 1168 – 1169.
[41] O. W. Webster, W. R. Hertler, D. Y. Sogah, W. B. Farnham, T. V. RajanBabu, *J. Am. Chem. Soc.* **1983**, *105*, 5706 – 5708.
[42] K. Matyjaszewski, J. Xia, *Chem. Rev.* **2001**, *101*, 2921 – 2990.
[43] M. Ouchi, T. Terashima, M. Sawamoto, *Chem. Rev.* **2009**, *109*, 4963 – 5050.
[44] J. Chiefari, Y. K. (Bill) Chong, F. Ercole, J. Krstina, J. Jeffery, T. P. T. Le, R. T. A. Mayadunne, G. F. Meijs, C. L. Moad, G. Moad, E. Rizzardo, S. H. Thang, *Macromolecules* **1998**, *31*, 5559 – 5562.
[45] A. B. Lowe, C. L. McCormick, *Prog. Polym. Sci.* **2007**, *32*, 283 – 351.
[46] C. J. Hawker, A. W. Bosman, E. Harth, *Chem. Rev.* **2001**, *101*, 3661 – 3688.
[47] M. K. Georges, R. P. N. Veregin, P. M. Kazmaier, G. K. Hamer, *Macromolecules* **1993**, *26*, 2987 – 2988.
[48] M. R. Buchmeiser, *Chem. Rev.* **2000**, *100*, 1565 – 1604.
[49] A. Leitgeb, J. Wappel, C. Slugovc, *Polymer* **2010**, *51*, 2927 – 2946.
[50] T. Humplik, J. Lee, S. C. O'Hern, B. A. Fellman, M. A. Baig, S. F. Hassan, M. A. Atieh, F. Rahman, T. Laoui, R. Karnik, E. N. Wang, *Nanotechnology* **2011**, *22*, 292001.
[51] D.-H. Choi, Y. D. Han, B.-K. Lee, S.-J. Choi, H. C. Yoon, D.-S. Lee, J.-B. Yoon, *Adv. Mater.* **2012**, *24*, 4408 – 4413.
[52] J. W. Colson, W. R. Dichtel, *Nat. Chem.* **2013**, *5*, 453 – 465.
[53] M. Kim, J. N. Hohman, Y. Cao, K. N. Houk, H. Ma, A. K.-Y. Jen, P. S. Weiss, *Science* **2011**, *331*, 1312 – 1315.
[54] B. Trappmann, J. E. Gautrot, J. T. Connelly, D. G. T. Strange, Y. Li, M. L. Oyen, M. A. Cohen Stuart, H. Boehm, B. Li, V. Vogel, J. P. Spatz, F. M. Watt, W. T. S. Huck, *Nat. Mater.* **2012**, *11*, 642 – 649.
[55] T. Rodenas, I. Luz, G. Prieto, B. Seoane, H. Miro, A. Corma, F. Kapteijn, F. X. Llabrés i Xamena, J. Gascon, *Nat. Mater.* **2015**, *14*, 48 – 55.
[56] K. Tahara, H. Yamaga, E. Ghijsens, K. Inukai, J. Adisoejoso, M. O. Blunt, S. De Feyter, Y. Tobe, *Nat. Chem.* **2011**, *3*, 714 – 719.
[57] J. Liu, Y. Liu, N. Liu, Y. Han, X. Zhang, H. Huang, Y. Lifshitz, S.-T. Lee, J. Zhong, Z. Kang, *Science* **2015**, *347*, 970 – 974.
[58] J. Sakamoto, J. van Heijst, O. Lukin, A. D. Schlüter, *Angew. Chem. Int. Ed.* **2009**, *48*, 1030 – 1069; *Angew. Chem.* **2009**, *121*, 1048 – 1089.
[59] P. Kissel, R. Erni, W. B. Schweizer, M. D. Rossell, B. T. King, T. Bauer, S. Götzinger, A. D. Schlüter, J. Sakamoto, *Nat. Chem.* **2012**, *4*, 287 – 291.
[60] For examples of 2D polymers with aperiodic bonding see: a) A. Küller, W. Eck, V. Stadler, W. Geyer, A. Gölzhäuser, *Appl. Phys. Lett.* **2003**, *82*, 3776 – 3778; b) S. Edmondson, W. T. S. Huck, *Adv. Mater.* **2004**, *16*, 1327 – 1331; c) K. Baek, G. Yun, Y. Kim, D. Kim, R. Hota, I. Hwang, D. Xu, Y. H. Ko, G. H. Gu, J. H. Suh, C. G. Park, B. J. Sung, K. Kim, *J. Am. Chem. Soc.* **2013**, *135*, 6523 – 6528; d) A. D. Stroock, R. S. Kane, M. Weck, S. J. Metallo, G. M. Whitesides, *Langmuir* **2003**, *19*, 2466 – 2472; e) M. J. Schultz, X. Zhang, S. Unarunotai, D.-Y. Khang, Q. Cao, C. Wang, C. Lei, S. MacLaren, J. A. N. T. Soares, I. Petrov, J. S. Moore, J. A. Rogers, *Proc. Natl. Acad. Sci. USA* **2008**, *105*, 7353 – 7358.
[61] J. W. Colson, A. R. Woll, A. Mukherjee, M. P. Levendorf, E. L. Spitler, V. B. Shields, M. G. Spencer, J. Park, W. R. Dichtel, *Science* **2011**, *332*, 228 – 231.
[62] For relevant earlier work see: a) A. P. Côté, A. I. Benin, N. W. Ockwig, M. O'Keeffe, A. J. Matzger, O. M. Yaghi, *Science* **2005**, *310*, 1166 – 1170; b) N. A. A. Zwaneveld, R. Pawlak, M. Abel, D. Catalin, D. Gigmes, D. Bertin, L. Porte, *J. Am. Chem. Soc.* **2008**, *130*, 6678 – 6679.
[63] L. Grill, M. Dyer, L. Lafferentz, M. Persson, M. V. Peters, S. Hecht, *Nat. Nanotechnol.* **2007**, *2*, 687 – 691.
[64] For relevant work see: a) S. Weigelt, C. Busse, C. Bombis, M. M. Knudsen, K. V. Gothelf, E. Lægsgaard, F. Besenbacher, T. R. Linderoth, *Angew. Chem. Int. Ed.* **2008**, *47*, 4406 – 4410; *Angew. Chem.* **2008**, *120*, 4478 – 4482; b) R. Tanoue, R. Higuchi, N. Enoki, Y. Miyasato, S. Uemura, N. Kimizuka, A. Z. Stieg, J. K. Gimzewski, M. Kunitake, *ACS Nano* **2011**, *5*, 3923 – 3929.
[65] M. Abel, S. Clair, O. Ourdjini, M. Mossoyan, L. Porte, *J. Am. Chem. Soc.* **2011**, *133*, 1203 – 1205.
[66] E. L. Spitler, B. T. Koo, J. L. Novotney, J. W. Colson, F. J. Uribe-Romo, G. D. Gutierrez, P. Clancy, W. R. Dichtel, *J. Am. Chem. Soc.* **2011**, *133*, 19416 – 19421.
[67] For examples of related work on 2D COFs see: a) L. Chen, K. Furukawa, J. Gao, A. Nagai, T. Nakamura, Y. Dong, D. Jiang, *J. Am. Chem. Soc.* **2014**, *136*, 9806 – 9809; b) S. Dalapati, S. Jin, J. Gao, Y. Xu, A. Nagai, D. Jiang, *J. Am. Chem. Soc.* **2013**, *135*, 17310 – 17313; c) S. Jin, K. Furukawa, M. Addicoat, L. Chen, S. Takahashi, S. Irle, T. Nakamura, D. Jiang, *Chem. Sci.* **2013**, *4*, 4505 – 4511; d) D. D. Medina, J. M. Rotter, Y. Hu, M. Dogru, V. Werner, F. Auras, J. T. Markiewicz, P. Knochel, T. Bein, *J. Am. Chem. Soc.* **2015**, *137*, 1016 – 1019; e) D. D. Medina, V. Werner, F. Auras, R. Tautz, M. Dogru, J. Schuster, S. Linke, M. Döblinger, J. Feldmann, P. Knochel, T. Bein, *ACS Nano* **2014**, *8*, 4042 – 4052.
[68] D. Bradshaw, S. El-Hankari, L. Lupica-Spagnolo, *Chem. Soc. Rev.* **2014**, *43*, 5431 – 5443.
[69] Q.-L. Zhu, Q. Xu, *Chem. Soc. Rev.* **2014**, *43*, 5468 – 5512.
[70] W. Lu, Z. Wei, Z.-Y. Gu, T.-F. Liu, J. Park, J. Park, J. Tian, M. Zhang, Q. Zhang, T. Gentle III, M. Bosch, H.-C. Zhou, *Chem. Soc. Rev.* **2014**, *43*, 5561 – 5593.
[71] S. Furukawa, J. Reboul, S. Diring, K. Sumida, S. Kitagawa, *Chem. Soc. Rev.* **2014**, *43*, 5700 – 5734.
[72] T. R. Cook, Y.-R. Zheng, P. J. Stang, *Chem. Rev.* **2013**, *113*, 734 – 777.
[73] D. Zacher, R. Schmid, C. Wöll, R. A. Fischer, *Angew. Chem. Int. Ed.* **2011**, *50*, 176 – 199; *Angew. Chem.* **2011**, *123*, 184 – 208.
[74] D. Zacher, O. Shekhah, C. Wöll, R. A. Fischer, *Chem. Soc. Rev.* **2009**, *38*, 1418 – 1429.
[75] J. Borges, J. F. Mano, *Chem. Rev.* **2014**, *114*, 8883 – 8942.
[76] R. Makiura, S. Motoama, Y. Umemura, H. Yamanaka, O. Sakata, H. Kitagawa, *Nat. Mater.* **2010**, *9*, 565 – 571.
[77] T. Bauer, Z. Zheng, A. Renn, R. Enning, A. Stemmer, J. Sakamoto, A. D. Schlüter, *Angew. Chem. Int. Ed.* **2011**, *50*, 7879 – 7884; *Angew. Chem.* **2011**, *123*, 8025 – 8030.
[78] T. Bauer, A. D. Schlüter, J. Sakamoto, *Synlett* **2010**, 877 – 880.
[79] M. E. Gallina, G. Bergamini, S. Di Motta, J. Sakamoto, F. Negri, P. Ceroni, *Photochem. Photobiol. Sci.* **2014**, *13*, 997 – 1004.
[80] Z. Zheng, C. S. Ruiz-Vargas, T. Bauer, A. Rossi, P. Payamyar, A. Schütz, A. Stemmer, J. Sakamoto, A. D. Schlüter, *Macromol. Rapid Commun.* **2013**, *34*, 1670 – 1680.
[81] Z. Zheng, L. Opilik, F. Schiffmann, W. Liu, G. Bergamini, P. Ceroni, L.-T. Lee, A. Schütz, J. Sakamoto, R. Zenobi, J. VandeVondele, A. D. Schlüter, *J. Am. Chem. Soc.* **2014**, *136*, 6103 – 6110.
[82] M. Bieri, M. Treier, J. Cai, K. Aït-Mansour, P. Ruffieux, O. Gröning, P. Gröning, M. Kastler, R. Rieger, X. Feng, K. Müllen, R. Fasel, *Chem. Commun.* **2009**, 6919 – 6921.
[83] M. Bieri, M.-T. Nguyen, O. Gröning, J. Cai, M. Treier, K. Aït-Mansour, P. Ruffieux, C. A. Pignedoli, D. Passerone, M. Kastler, K. Müllen, R. Fasel, *J. Am. Chem. Soc.* **2010**, *132*, 16669 – 16676.
[84] J. Zhou, Q. Sun, *J. Am. Chem. Soc.* **2011**, *133*, 15113 – 15119.
[85] T. Kambe, R. Sakamoto, K. Hoshiko, K. Takada, M. Miyachi, J.-H. Ryu, S. Sasaki, J. Kim, K. Nakazato, M. Takata, H. Nishihara, *J. Am. Chem. Soc.* **2013**, *135*, 2462 – 2465.

[86] T. Kambe, R. Sakamoto, T. Kusamoto, T. Pal, N. Fukui, K. Hoshiko, T. Shimojima, Z. Wang, T. Hirahara, K. Ishizaka, S. Hasegawa, F. T. Liu, H. Nishihara, *J. Am. Chem. Soc.* **2014**, *136*, 14357 – 14360.
[87] J. Moore, *Nat. Phys.* **2009**, *5*, 378 – 380.
[88] T. M. Long, T. M. Swager, *Adv. Mater.* **2001**, *13*, 601 – 604.
[89] R. Bhola, P. Payamyar, D. J. Murray, B. Kumar, A. J. Teator, M. U. Schmidt, S. M. Hammer, A. Saha, J. Sakamoto, A. D. Schlüter, B. T. King, *J. Am. Chem. Soc.* **2013**, *135*, 14134 – 14141.
[90] G. W. Breton, X. Vang, *J. Chem. Educ.* **1998**, *75*, 81 – 82.
[91] P. Payamyar, K. Kaja, C. Ruiz-Vargas, A. Stemmer, D. J. Murray, C. J. Johnson, B. T. King, F. Schiffmann, J. VandeVondele, A. Renn, S. Götzinger, P. Ceroni, A. Schütz, L. T. Lee, Z. Zheng, J. Sakamoto, A. D. Schlüter, *Adv. Mater.* **2014**, *26*, 2052 – 2058.
[92] P. Kissel, J. Van Heijst, R. Enning, A. Stemmer, A. D. Schlüter, J. Sakamoto, *Org. Lett.* **2010**, *12*, 2778 – 2781.
[93] P. Kissel, D. J. Murray, W. J. Wulftange, V. J. Catalano, B. T. King, *Nat. Chem.* **2014**, *6*, 774 – 778.
[94] M. Kory, M. Wörle, T. Weber, P. Payamyar, S. W. van de Poll, J. Dshemuchadse, N. Trapp, A. D. Schlüter, *Nat. Chem.* **2014**, *6*, 779 – 784.
[95] P. Podsiadlo, A. K. Kaushik, E. M. Arruda, A. M. Waas, B. S. Shim, J. Xu, H. Nandivada, B. G. Pumplin, J. Lahann, A. Ramamoorthy, N. A. Kotov, *Science* **2007**, *318*, 80 – 83.
[96] X. Li, W. Cai, J. An, S. Kim, J. Nah, D. Yang, R. Piner, A. Velamakanni, I. Jung, E. Tutuc, S. K. Banerjee, L. Colombo, R. S. Ruoff, *Science* **2009**, *324*, 1312 – 1314.
[97] J.-W. Seo, Y.-W. Jun, S.-W. Park, H. Nah, T. Moon, B. Park, J.-G. Kim, Y. J. Kim, J. Cheon, *Angew. Chem. Int. Ed.* **2007**, *46*, 8828 – 8831; *Angew. Chem.* **2007**, *119*, 8984 – 8987.
[98] X. Ye, J. Chen, M. Engel, J. A. Millan, W. Li, L. Qi, G. Xing, J. E. Collins, C. R. Kagan, J. Li, S. C. Glotzer, C. B. Murray, *Nat. Chem.* **2013**, *5*, 466 – 473.
[99] W.-B. Zhang, X. Yu, C.-L. Wang, H.-J. Sun, I.-F. Hsieh, Y. Li, X.-H. Dong, K. Yue, R. Van Horn, S. Z. D. Cheng, *Macromolecules* **2014**, *47*, 1221 – 1239.
[100] M. O. Blunt, J. C. Russell, M. D. C. Giménez-López, J. P. Garrahan, X. Lin, M. Schröder, N. R. Champness, P. H. Beton, *Science* **2008**, *322*, 1077 – 1081.
[101] J. Carrasco, A. Michaelides, M. Forster, S. Haq, R. Raval, A. Hodgson, *Nat. Mater.* **2009**, *8*, 427 – 431.
[102] S. Haq, F. Hanke, J. Sharp, M. Persson, D. B. Amabilino, R. Raval, *ACS Nano* **2014**, *8*, 8856 – 8870.
[103] M. P. Boneschanscher, W. H. Evers, J. J. Geuchies, T. Altantzis, B. Goris, F. T. Rabouw, S. A. P. van Rossum, H. S. J. van der Zant, L. D. A. Siebbeles, G. Van Tendeloo, I. Swart, J. Hilhorst, A. V. Petukhov, S. Bals, D. Vanmaekelbergh, *Science* **2014**, *344*, 1377 – 1380.
[104] X. Ye, J. E. Collins, Y. Kang, J. Chen, D. T. N. Chen, A. G. Yodh, C. B. Murray, *Proc. Natl. Acad. Sci. USA* **2010**, *107*, 22430 – 22435.
[105] Y. Li, W.-B. Zhang, I.-F. Hsieh, G. Zhang, Y. Cao, X. Li, C. Wesdemiotis, B. Lotz, H. Xiong, S. Z. D. Cheng, *J. Am. Chem. Soc.* **2011**, *133*, 10712 – 10715.
[106] H.-J. Sun, Y. Tu, C.-L. Wang, R. M. Van Horn, C.-C. Tsai, M. J. Graham, B. Sun, B. Lotz, W.-B. Zhang, S. Z. D. Cheng, *J. Mater. Chem.* **2011**, *21*, 14240 – 14247.
[107] P.-G. de Gennes, *Angew. Chem. Int. Ed. Engl.* **1992**, *31*, 842 – 845; *Angew. Chem.* **1992**, *104*, 856 – 859.
[108] H. Liu, C. Hsu, Z. Lin, W. Shan, J. Wang, J. Jiang, M. Huang, B. Lotz, X. Yu, W.-B. Zhang, K. Yue, S. Z. D. Cheng, *J. Am. Chem. Soc.* **2014**, *136*, 10691 – 10699.
[109] H. Shin, K. S. Schweizer, *Soft Matter* **2014**, *10*, 262 – 274.
[110] C. Bouet, B. Mahler, B. Nadal, B. Abecassis, M. D. Tessier, S. Ithurria, X. Xu, B. Dubertret, *Chem. Mater.* **2013**, *25*, 639 – 645.
[111] H. Li, J. Wu, Z. Yin, H. Zhang, *Acc. Chem. Res.* **2014**, *47*, 1067 – 1075.
[112] X. Huang, Z. Zeng, H. Zhang, *Chem. Soc. Rev.* **2013**, *42*, 1934 – 1946.
[113] C. Tan, H. Zhang, *Chem. Soc. Rev.* **2015**, *44*, 2713 – 2731.
[114] X. Huang, C. Tan, Z. Yin, H. Zhang, *Adv. Mater.* **2014**, *26*, 2185 – 2204.
[115] C. Tan, X. Qi, X. Huang, J. Yang, B. Zheng, Z. An, R. Chen, J. Wei, B. Z. Tang, W. Huang, H. Zhang, *Adv. Mater.* **2014**, *26*, 1735 – 1739.
[116] Y. Zhong, Y. Yang, Y. Ma, J. Yao, *Chem. Commun.* **2013**, *49*, 10355 – 10357.
[117] S. Acharya, B. Das, U. Thupakula, K. Ariga, D. D. Sarma, J. Israelachvili, Y. Golan, *Nano Lett.* **2013**, *13*, 409 – 415.
[118] X. Hong, C. Tan, J. Liu, J. Yang, X.-J. Wu, Z. Fan, Z. Luo, J. Chen, X. Zhang, B. Chen, H. Zhang, *J. Am. Chem. Soc.* **2015**, *137*, 1444 – 1447.
[119] K. Taguchi, H. Miyaji, K. Izumi, A. Hoshino, Y. Miyamoto, R. Kokawa, *Polymer* **2001**, *42*, 7443 – 7447.
[120] N. Grozev, I. Botiz, G. Reiter, *Eur. Phys. J. E* **2008**, *27*, 63 – 71.
[121] G. Reiter, J.-U. Sommer, *Phys. Rev. Lett.* **1998**, *80*, 3771 – 3774.
[122] D. J. Blundell, A. Keller, A. J. Kovacs, *J. Polym. Sci. B* **1966**, *4*, 481 – 486.
[123] J. Xu, Y. Ma, W. Hu, M. Rehahn, G. Reiter, *Nat. Mater.* **2009**, *8*, 348 – 353.
[124] B. Li, B. Wang, R. C. M. Ferrier, C. Y. Li, *Macromolecules* **2009**, *42*, 9394 – 9399.
[125] S. E. Lohse, C. J. Murphy, *J. Am. Chem. Soc.* **2012**, *134*, 15607 – 15620.
[126] B. Dong, D. L. Miller, C. Y. Li, *J. Phys. Chem. Lett.* **2012**, *3*, 1346 – 1350.
[127] B. Dong, T. Zhou, H. Zhang, C. Y. Li, *ACS Nano* **2013**, *7*, 5192 – 5198.
[128] K. T. Nam, S. A. Shelby, P. H. Choi, A. B. Marciel, R. Chen, L. Tan, T. K. Chu, R. A. Mesch, B.-C. Lee, M. D. Connolly, C. Kisielowski, R. N. Zuckermann, *Nat. Mater.* **2010**, *9*, 454 – 460.
[129] Y. Zheng, H. Zhou, D. Liu, G. Floudas, M. Wagner, K. Koynov, M. Mezger, H.-J. Butt, T. Ikeda, *Angew. Chem. Int. Ed.* **2013**, *52*, 4845 – 4848; *Angew. Chem.* **2013**, *125*, 4945 – 4948.
[130] Molecular surfactants also form 2D structures, including the well-known bilayers as well as other planar aggregates; see, for example, G. Wu, J. Thomas, M. Smet, Z. Wang, X. Zhang, *Chem. Sci.* **2014**, *5*, 3267 – 3274, and references therein.
[131] L. Zhang, A. Eisenberg, *Science* **1995**, *268*, 1728 – 1731.
[132] Y. Mai, A. Eisenberg, *Chem. Soc. Rev.* **2012**, *41*, 5969 – 5985.
[133] J. Zhang, X.-F. Chen, H.-B. Wei, X.-H. Wan, *Chem. Soc. Rev.* **2013**, *42*, 9127 – 9154.
[134] A. P. Gast, P. K. Vinson, K. A. Cogan-Harinast, *Macromolecules* **1993**, *26*, 1774 – 1776.
[135] T. Vilgis, A. Halperin, *Macromolecules* **1991**, *24*, 2090 – 2095.
[136] B. Lotz, A. J. Kovacs, G. A. Bassett, A. Keller, *Kolloid Z. Z. Polym.* **1966**, *209*, 115 – 128.
[137] B. Lotz, A. J. Kovacs, *Kolloid Z. Z. Polym.* **1966**, *209*, 97 – 114.
[138] A. O. Moughton, M. A. Hillmyer, T. P. Lodge, *Macromolecules* **2012**, *45*, 2 – 19.
[139] D. E. Discher, A. Eisenberg, *Science* **2002**, *297*, 967 – 973.
[140] N. Petzetakis, A. P. Dove, R. K. O′Reilly, *Chem. Sci.* **2011**, *2*, 955 – 960.
[141] X. Wang, G. Guerin, H. Wang, Y. Wang, I. Manners, M. A. Winnik, *Science* **2007**, *317*, 644 – 647.
[142] J. B. Gilroy, T. Gädt, G. R. Whittell, L. Chabanne, J. M. Mitchels, R. M. Richardson, M. A. Winnik, I. Manners, *Nat. Chem.* **2010**, *2*, 566 – 570.
[143] L. Cao, I. Manners, M. A. Winnik, *Macromolecules* **2002**, *35*, 8258 – 8260.
[144] J. Wang, W. Zhu, B. Peng, Y. Chen, *Polymer* **2013**, *54*, 6760 – 6767.

[145] Z. M. Hudson, C. E. Boott, M. E. Robinson, P. A. Rupar, M. A. Winnik, I. Manners, *Nat. Chem.* **2014**, *6*, 893 – 898.
[146] B. Yu, X. Jiang, J. Yin, *Macromolecules* **2014**, *47*, 4761 – 4768.
[147] S. F. M. Yusoff, M.-S. Hsiao, F. H. Schacher, M. A. Winnik, I. Manners, *Macromolecules* **2012**, *45*, 3883 – 3891.
[148] M.-S. Hsiao, S. F. M. Yusoff, M. A. Winnik, I. Manners, *Macromolecules* **2014**, *47*, 2361 – 2372.
[149] M. Su, H. Huang, X. Ma, Q. Wang, Z. Su, *Macromol. Rapid Commun.* **2013**, *34*, 1067 – 1071.
[150] G. Rizis, T. G. M. van de Ven, A. Eisenberg, *Angew. Chem. Int. Ed.* **2014**, *53*, 9000 – 9003; *Angew. Chem.* **2014**, *126*, 9146 – 9149.
[151] G. Rizis, T. G. M. van de Ven, A. Eisenberg, *Soft Matter* **2014**, *10*, 2825 – 2835.
[152] T. Gädt, N. S. Ieong, G. Cambridge, M. A. Winnik, I. Manners, *Nat. Mater.* **2009**, *8*, 144 – 150.
[153] J. Qian, Y. Lu, A. Chia, M. Zhang, P. A. Rupar, N. Gunari, G. C. Walker, G. Cambridge, F. He, G. Guerin, I. Manners, M. A. Winnik, *ACS Nano* **2013**, *7*, 3754 – 3766.
[154] J. Qian, G. Guerin, Y. Lu, G. Cambridge, I. Manners, M. A. Winnik, *Angew. Chem. Int. Ed.* **2011**, *50*, 1622 – 1625; *Angew. Chem.* **2011**, *123*, 1660 – 1663.
[155] Z. M. Hudson, D. J. Lunn, M. A. Winnik, I. Manners, *Nat. Commun.* **2014**, *5*, 3372.
[156] J. R. Finnegan, D. J. Lunn, O. E. C. Gould, Z. M. Hudson, G. R. Whittell, M. A. Winnik, I. Manners, *J. Am. Chem. Soc.* **2014**, *136*, 13835 – 13844.
[157] C. Sinturel, M. Vayer, R. Erre, H. Amenitsch, *Eur. Polym. J.* **2009**, *45*, 2505 – 2512.
[158] R. M. Erb, R. Libanori, N. Rothfuchs, A. R. Studart, *Science* **2012**, *335*, 199 – 204.
[159] L. J. Bonderer, A. R. Studart, L. J. Gauckler, *Science* **2008**, *319*, 1069 – 1073.
[160] D. Gournis, G. Floudas, *Chem. Mater.* **2004**, *16*, 1686 – 1692.
[161] B. Yu, X. Jiang, J. Yin, *Chem. Commun.* **2013**, *49*, 603 – 605.
[162] A. Presa Soto, J. B. Gilroy, M. A. Winnik, I. Manners, *Angew. Chem. Int. Ed.* **2010**, *49*, 8220 – 8223; *Angew. Chem.* **2010**, *122*, 8396 – 8399.
[163] W. Y. Chen, C. Y. Li, J. X. Zheng, P. Huang, L. Zhu, Q. Ge, R. P. Quirk, B. Lotz, L. Deng, C. Wu, E. L. Thomas, S. Z. D. Cheng, *Macromolecules* **2004**, *37*, 5292 – 5299.
[164] J. Zhu, S. Zhang, K. Zhang, X. Wang, J. W. Mays, K. L. Wooley, D. J. Pochan, *Nat. Commun.* **2013**, *4*, 2297.
[165] P. A. Rupar, L. Chabanne, M. A. Winnik, I. Manners, *Science* **2012**, *337*, 559 – 562.
[166] H. Wang, W. Lin, K. P. Fritz, G. D. Scholes, M. A. Winnik, I. Manners, *J. Am. Chem. Soc.* **2007**, *129*, 12924 – 12925.
[167] R. F. Service, *Science* **2015**, *348*, 490 – 492.
[168] J. S. Guevara, A. F. Mejia, M. Shuai, Y.-W. Chang, M. S. Mannan, Z. Cheng, *Soft Matter* **2013**, *9*, 1327 – 1336.
[169] P. Decuzzi, B. Godin, T. Tanaka, S.-Y. Lee, C. Chiappini, X. Liu, M. Ferrari, *J. Controlled Release* **2010**, *141*, 320 – 327.
[170] C. Tschierske, D. J. Photinos, *J. Mater. Chem.* **2010**, *20*, 4263 – 4294.

Received: March 3, 2015
Revised: May 18, 2015
Published online: October 22, 2015